The Pennsylvania State University

The Graduate School

Department of Electrical Engineering

EVOLUTION OF OZONE AND PARTCULATE MATTER DURING POLLUTION EVENTS USING RAMAN LIDAR

A Thesis in

Electrical Engineering

by

Karoline R. Mulik

Submitted in Partial Fulfillment
of the Requirements
for the Degree of

Master of Science

May 2000

I grant The Pennsylvania State University the nonexclusive right to use this work for the University's own purposes and to make single copies of the work available to the public on a not-for-profit basis if copies are not otherwise available.

_____

Karoline R. Mulik

We approve the thesis of Karoline R. Mulik.

Date of Signature

_____ _____

C. Russell Philbrick
Professor of Electrical Engineering
Thesis Advisor

_____ _____

Iam-Choon Khoo
Professor of Electrical Engineering

_____ _____

Sven Bilén
Assistant Professor of Electrical Engineering

_____ _____

Kenneth Jenkins
Professor of Electrical Engineering
Head of the Department of Electrical Engineering

Abstract

An investigation of air pollution episodes using remote sensing provided a means of describing the impact of local meteorology on the development and dissipation of air pollution events. Lidar was used to measure atmospheric constituents and provided a continuous monitor of the lower atmosphere's vertical structure during the NARSTO-NE-OPS (North American Research Strategy for Tropospheric Ozone - North East - Oxidant and Particle Study). The NE-OPS study was conducted in the Philadelphia urban environment where a combination of pollution sources exists. The PSU Lidar Atmospheric Profile Sensor (LAPS) instrument measured ozone, water vapor, temperature, optical backscatter, and extinction, and the Science and Engineering Services, Inc. Micro Pulse Lidar (MPL) measured backscatter. LAPS transmits a laser beam and measures the scattered radiation at several wavelengths of Raman scattered signals using multi-channel photon counting detection, and provides vertical profiles of atmospheric properties. The MPL provides vertical profiles of backscatter signal. Analysis of an interesting pollution episode that occurred on 21 August 1998 was performed, which exhibited the dramatic effects associated with pollutant precursor material transportation and temperature dependence. Time sequences of water vapor depict an aloft plume mixing downward into the rising convective boundary layer, which resulted in simultaneous increases of backscatter, extinction, and ozone at the surface. Surface ozone concentrations reached approximately 120 ppb in a short period of three hours, and particle scattering extinction values at 284 nm reached 3 km^{-1}. A possible transport reservoir of the ozone precursors responsible for these increases is thought to be

peroxyacetyl nitrate (PAN), which has a thermal dissociation rate that increases exponentially. Results from this episode demonstrate the importance of vertical mixing, horizontal transport, and storage of precursor and pollutant matter.

Table of Contents

List of Figures

List of Tables

Acknowledgments

I would like to thank my advisor, Professor C. Russell Philbrick, for his support and guidance through my research and academics. His encouragement and advice helped give me the confidence to accomplish more than I thought. I would also like to thank my committee members, Dr. I.C. Khoo and Dr. Sven Bilén, for their support and recommendations.

Thanks are also due to Dr. Dan Lysak, Tom Petach, Dr. Derrek Dunn, Edie S. Sears, Ed Novitsky, Alex Achey, Guankun Li, Ginnipal Chadha, James Carbo, Gregg O'Marr, and especially Steven Esposito. The efforts of Mr. George Allen of Harvard University School of Public Health, Drs. Russell Dickerson, Bruce Doddridge, and William Ryan of University of Maryland, Dr. Richard Clark of Millersville University, Dr. S.T. Rao of NY State Dept. of Environmental Conservation, Mr. William Miller of Philadelphia-AMS, Mr. Ted Erdman of EPA Region 3, Drs. Sharon LeDuc, and Francis Binkowski of USEPA have contributed much to the success of this project.

I would also like to thank my family and friends for their encouragement and understanding. Their love and support helped me throughout my studies and encouraged me to achieve my goals.

CHAPTER 1

Introduction

Determining atmospheric trends of airborne particulate matter requires investigations of the sources of ozone and fine aerosol particles, their origins in a range of processes from chemical generation to mechanical injection, and their distribution and control by meteorological processes. We must understand the short and long-term impact of urban and industrial activities on the environment, so that developments can be made to lessen the harmful effects. Scientific investigations provide an opportunity to study pollutant formation and transportation, as well as how these pollutants affect air quality, visibility, global climate, and population exposure. Injection and transport of chemical precursors of atmospheric pollutants significantly expand the regional scales of concern in describing the concentrations of emissions that result in pollution.

Ozone in the lower atmosphere is formed primarily through photochemical reactions, but transport of ozone and its chemical precursors from outside regions is also a large contributor to the total surface ozone concentration. However, the exact location of the ozone and particulate matter precursors origin can be difficult to determine. At times, the important species originates from local sources, such as nitrates from internal combustion engines and sulfates emanating from power plants, factories, and diesel fuel combustion, or they could be transported from outlying regions and mixed to the surface causing chemical reactions, which result in formation of ozone. This is very interesting because the transported precursors could also result in aerosol haze, thus showing that an increase in particulate matter could occur simultaneously with an increase in ozone. The

formation of both ozone and particulate matter (PM) are very closely correlated, and investigations of them should be considered together, since they are both greatly influenced by meteorological factors, as well as some source common factors in their generation. The correlation of profiles of optical extinction from particulate matter with profiles of water vapor and ozone in the atmosphere provides extremely important insight to understanding the evolution of pollution events.

Examination of pollution episodes is essential for understanding their impact on air quality, as well as determining how the meteorology and dynamics of the lower atmosphere affect pollution trends. The data to be presented in this thesis were taken as part of the North-East Oxidant and Particle Study (NE-OPS) pilot campaign during a two-week period in August 1998 [Philbrick, 1998]. The main objectives of the NE-OPS campaign are to understand pollution sources and the controlling meteorological processes that cause increased air pollutant concentrations on local and regional scales and to provide vital data for testing and improving modeling of conditions when pollution episodes occur [Philbrick, 1998]. Data was obtained in an urban environment, where there is a combination of local sources, as well as contributions from distant sources. The measurement site was located in Philadelphia, PA, approximately 14 km northwest of the center of the city. Measurements were made using several different instruments by a consortium of university and government laboratory participants. The Pennsylvania State University's Department of Electrical Engineering contributed measurements of vertical profiles of atmospheric constituents using a multi-wavelength Raman lidar to describe these pollution events in the lower atmosphere. Raman lidar is a remote sensing technique that uses a laser at a certain wavelength to transmit at an intense pulse of

optical radiation and measures the Raman-shifted backscatter of photons from molecules. The signal profiles from Raman scatter wavelengths at 607, 530, and 284 nm and the lidar backscatter at 532 nm were used to measure optical properties, while at the same time Raman lidar measurements of water vapor, temperature, and ozone profiles were obtained. Backscatter profiles were also obtained using a Micro Pulse Lidar and then compared with other measurements. Lidar provides an important means of measuring atmospheric data because it has the capability of continuous, autonomous measurement and provides times sequences of data that can be used to describe the vertical and horizontal structure of the lower atmosphere. The lidar measurements from this pilot study were used to describe the dynamics of the atmosphere and provide information about atmospheric constituents.

This thesis will provide a description of the Raman lidar measurement technique, and an analysis of data obtained during a pollution event using this state-of-the-art remote sensing method. The methods of measurement and data processing techniques using data obtained from the PSU Lidar Atmospheric Profile Sensor instrument will be discussed. Interesting data showing the transport of ozone precursors and the downward mixing to rapidly produce ozone at the surface will be examined. The relationship of ozone and particulate matter will be investigated and displayed using the vertical time sequence profiles obtained by the lidars. Comparisons with local aircraft spirals and tethersonde data were made for verification of the various measurement techniques.

CHAPTER 2

Lidar Measurement Techniques

2.1 Introduction

Optical remote sensing provides a meaningful method of studying the atmosphere and its constituents using molecular Raman scattering. The remote sensing instrument that is utilized for these studies is lidar, which is the acronym for LIght Detection And Ranging and is commonly referred to as laser radar. A lidar system transmits a laser beam at a certain wavelength into the atmosphere, and a telescope collects the return signals, including direct backscatter, vibrational Raman and rotational Raman signals, at different wavelengths using a detection system. The return signals are then analyzed to obtain measurements of atmospheric constituents.

2.2 Raman Scattering

Raman lidar utilizes the signals from Raman inelastic scattering by atmospheric molecules. Raman inelastic scattering occurs when laser irradiation is scattered by molecules at energy differences associated with the vibrational and rotational energy states of the molecules [Measures, 1984]. This shift in frequency of the scattered photon is due to the energy difference between the incident and scattered photons that is characteristic of the vibrational and rotational energy states of each molecule. If the resulting radiation has a longer wavelength, or lower frequency, the molecule has gained energy, and the scattered radiation is referred to as the Stokes component. If the molecule loses energy, the scattered radiation (red shifted) is referred to as the anti-

Stokes component [Measures, 1984]. The energy shift of the Stokes and anti-Stokes components are shown in Figure 2.1.

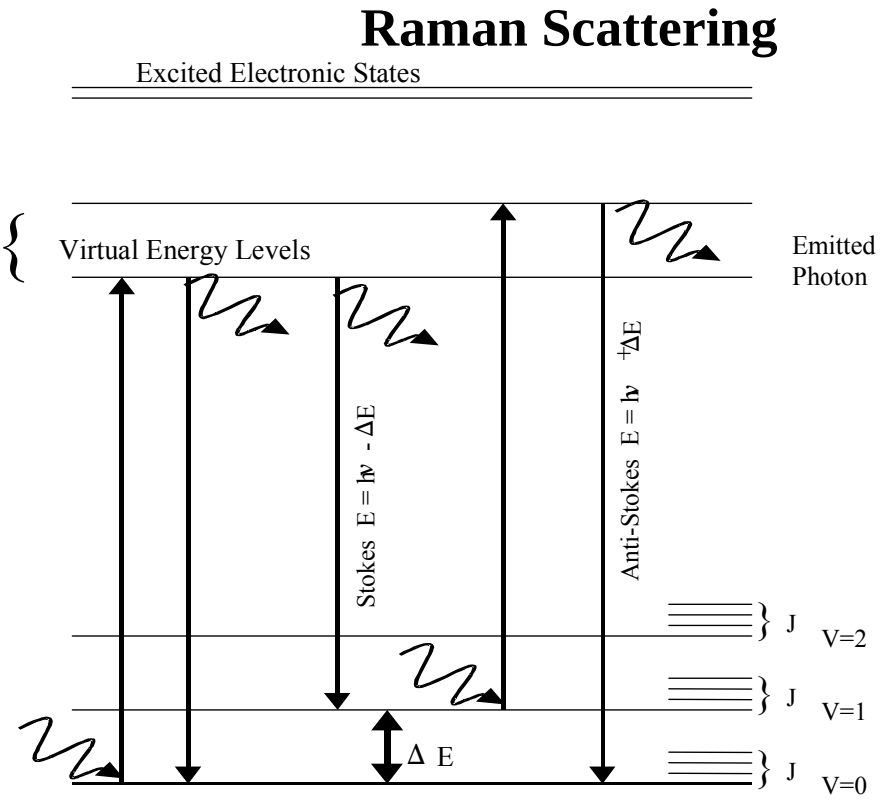

Figure 2.1. Stokes and anti-Stokes energy shifts are shown that schematically represent Raman scattering theory.

The Raman spectrum consists of vibrational states and their associated rotational states. Typically, Raman measurements of an atmospheric species are measured as a signal ratio to a specific molecule which represents the total density, such as N_2 or O_2, since this provides a direct measurement of the relative concentration of the species [Measures, 1984]. The vibrational and rotational Raman signals using a 532 nm laser are shown in Figure 2.2 [Philbrick, 1994].

Our ability to measure the Raman-shifted radiation of these molecules is very useful for pollution monitoring. The intensity of a Raman signal is directly proportional to the density of the scattered molecule and independent of other scattered molecules [Measures, 1984]. The wavelength shift and narrow spectral width of the Raman return signal allows it to be distinguished from solar background radiation and other sources of elastically scattered radiation [Measures, 1984]. These characteristics of Raman lidar make it a very powerful tool in accurately measuring atmospheric constituents such as water vapor and ozone.

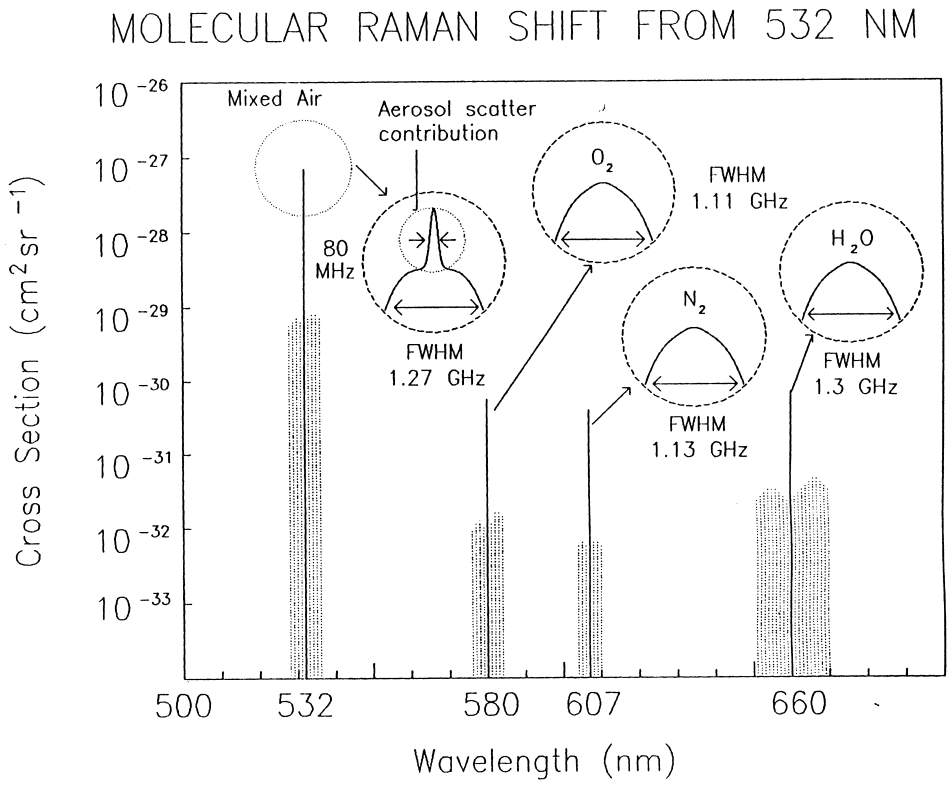

Figure 2.2. Relative sensitivity is indicated by the cross-section of vibrational and rotational Raman shifts for O_2, N_2, H_2O, and aerosol scatter for a 532-nm laser transmitter [Philbrick, 1994].

2.3 Lidar Atmospheric Profile Sensor Instrument

Measurements presented in this thesis were made during the 1998 North-East Oxidant and Particle Study (NE-OPS) pilot study in Philadelphia, PA, using the Pennsylvania State University/ARL lidar, referred to as LAPS (Lidar Atmospheric Profile Sensor) [Philbrick, 1998], and the Science and Engineering Services, Inc., Micro Pulse Lidar [Lee, 1996]. LAPS was the primary instrument for measurements of vertical profiles of water vapor, extinction, and ozone during the 1998 campaign. It was originally designed as a rugged prototype instrument for the U.S. Navy to obtain RF refractivity measurements in a severe environment and has several useful features such as environmental control and real time data display/transfer of profiles of atmospheric properties [Esposito, 1998; Philbrick, 1994; Philbrick, 1998]. LAPS is a multi-wavelength Raman lidar that can take measurements during the daytime and nighttime under a wide range of weather conditions and can operate autonomously [Philbrick, 1994; Philbrick, 1998].

The LAPS instrument consists of a console and a deck unit, which are connected by fiber optic cables [Balsiger, et. al., 1996]. The main components of the deck unit are a Nd:YAG laser, beam expander telescope, the collecting telescope, and the fiber optic [Balsiger, et. al., 1996; Philbrick, 1998]. The Nd:YAG laser is pulsed at 30 Hz with an output power of 1.6 joules per pulse at the fundamental wavelength, 1064 nm. The 1064-nm laser beam is sent through two frequency-doubling harmonic crystals to transmit at wavelengths of 532 nm (2^{nd} harmonic) and 266 nm (4^{th} harmonic), and the radiation at these two wavelengths is scattered by molecules in the atmosphere. The output energy of the laser is not eye-safe, so several safety precautions must be taken during operation. A

radar with a six-degree cone angle around the vertical laser beam is used to detect aircraft and send a signal to shut off the beam if detection occurs. The transmission system characteristics of LAPS are given in Table 2.1 [Durbin, 1997; Philbrick, 1998].

Table 2.1. LAPS Transmitter Characteristics

Laser	Continuum Model 9030 with 5X Beam Expander
Pulse Frequency	30 Hz
Pulse Duration	8 ns
Fundamental Power	1.6 J/Pulse
Power Output at 1064 nm	Dumped into heat sink
Power Output at 532 nm	600 mJ
Power Output at 266 nm	130 mJ

The return signal is collected in an upward pointing telescope and focused onto a 1-mm fiber. The LAPS transmitter and receiver system configuration is shown in Figure 2.3 [Durbin, 1997; Jeness, 1997].

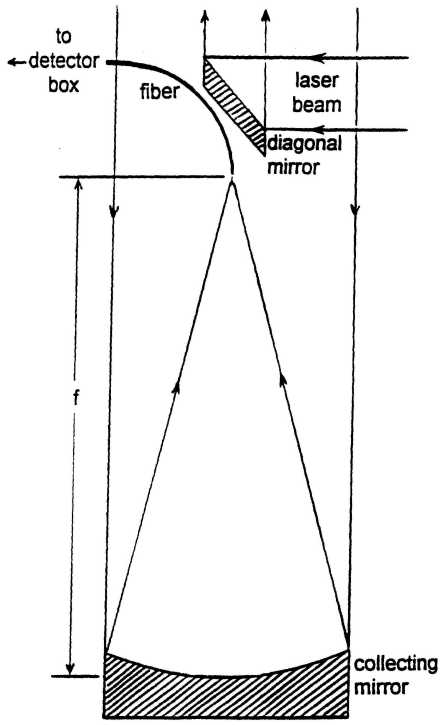

Figure 2.3. LAPS transmitter and receiver system components are shown [Jeness, 1997].

The return signal is then transferred by a fiber optic cable to a detector box in the console unit, which contains eight filters (each at a different wavelength), steering optics, lenses, and eight photomultiplier tubes (PMT's). Seven of the filters are set at the vibrational and rotational Raman-shifted wavelengths from the transmitted wavelengths at 532 nm and 266 nm to measure different molecules, and the last filter is set at 532 nm to measure backscatter. The signal from the fiber optic cable is split and filtered for each of the different Raman scatter wavelengths. The optical signals are then transferred to each corresponding PMT for photon counting. Due to the low Raman scatter cross-sections, the scattered photons are few in number, so high-sensitivity photomultipliers using photon-counting techniques for detection are needed. For optimal detection performance of the Raman signals, the PMT's need high collection efficiency, high gain, good multiplication statistics, low noise, and high photocathode quantum efficiency over the spectral range of interest. The detector box with the steering optics and each PMT channel can be seen in Figure 2.4.

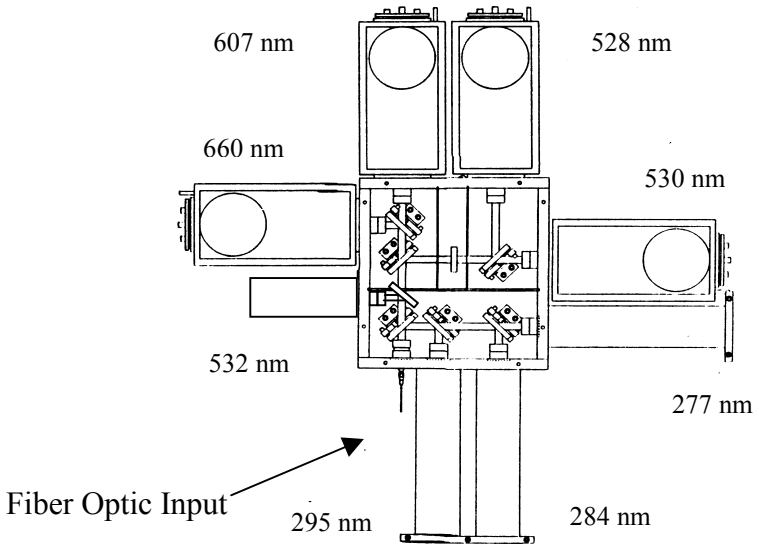

Figure 2.4. LAPS detector box is shown with the steering optics and the layout of each PMT.

The console provides the control for operation of the instrument and provides the data collection and display. It contains two PC's, the command computer and the display computer, a data acquisition system, and the detector box. The command computer sends control signals to the deck unit computer for instrument operation and receives signals back that confirm the transmitted control data. The data acquisition system transfers the data signals, as photon counts detected by the PMT's, to the command computer for processing. Data analysis programs on the command computer also provide output files of the photon counts. LAPS has a vertical resolution of 75 meters for seven of the PMT's and a vertical resolution of 3 meters for the backscatter PMT. The display computer processes the data files on the command computer and further utilizes the lidar scatter equations to display real-time vertical profiles of the water vapor, ozone, temperature, and extinction. Table 2.2 displays a summary of the features of LAPS.

Table 2.2. Summary of LAPS Features

Transmitter	Continuum 9030 –30 Hz 5X Beam Expander	600 mJ @ 532 nm 130 mJ @ 266 nm
Receiver	61 cm Diameter Telescope Focal length – 1.5 m	Fiber optic transfer
Detector	Eight PMT channels Photon Counting	660 and 607 nm – Water Vapor 528 and 530 nm – Temperature 295 and 284 nm – Daytime Water Vapor 277 and 284 nm – Raman/DIAL Ozone 607, 530, and 284 nm – Extinction 532 nm – Backscatter
Data System	DSP 100 MHz	75-meter range bins
Safety Radar	Marine R-70 X-Band	Protects 6° cone angle around beam

2.4 Measurement Techniques

The LAPS system uses Raman scattering techniques to measure vertical profiles of aerosol extinction, water vapor, temperature, and ozone. Rotational Raman scatter is

used to measure temperature, whereas vibrational Raman scattering is used to measure profiles of water vapor, ozone, and optical extinction. LAPS is able to detect the Raman shifts of several selected molecules using different channels. The vibrational and rotational Raman signals are measured for the 532-nm transmitted wavelength (refer to Figure 2.2 and Table 2.2) and for the 266-nm transmitted wavelength. The raw data obtained in photon counts provides information about the concentrations of N_2, O_2, and H_2O at different altitudes. These measurements can be interpreted using the basic lidar scattering equation and variations of it. The lidar scattering equation can be described by the power of the signal received by a monostatic lidar denoted by $P(\lambda_R,z)$, given by [Esposito, 1999; Measures, 1984]:

$$P(\lambda_R, z) = E_T(\lambda_T)\xi_T(\lambda_T)\xi_R(\lambda_R)\frac{c\tau}{2}\frac{A}{z^2}\beta(\lambda_T, \lambda_R)\exp\left[-\int_0^z [\alpha(\lambda_T, z') + \alpha(\lambda_R, z')]dz'\right] , \qquad [2.1]$$

where,

z	is the altitude of the volume element where the return signal is scattered,
λ_T	is the wavelength of the laser light transmitted,
λ_R	is the wavelength of the laser light received,
$E_T(\lambda_T)$	is the light energy per laser pulse transmitted at wavelength λ_T,
$\xi_T(\lambda_T)$	is the net optical efficiency at wavelength λ_T of all transmitting devices,
$\xi_R(\lambda_R)$	is the net optical efficiency at wavelength λ_R of all receiving devices,
c	is the speed of light,
τ	is the time duration of the laser pulse,
A	is the area of the receiving telescope,
$\beta(\lambda_T,\lambda_R)$	is the back scattering cross section of the volume scattering element for the laser wavelength λ_T at Raman shifted wavelength λ_R,
$\alpha(\lambda,z')$	is the extinction coefficient at wavelength λ at range z'.

This equation is used to interpret the signal returned in photon counts, so that vertical measurements of atmospheric components can be determined. The term $\xi_R(\lambda_R)$ is

important due to the geometrical considerations affecting it. $\xi_R(\lambda_R)$ is commonly known as the geometrical form factor and is assumed to be determined in the far field [Measures, 1984]. The analysis of the near field data (<800 m) must also be considered carefully, because overfilling of the detector causes the effective profile of the received signal to be distorted [Mulik, et. al., 2000]. One method of correcting for the signal distortion in the near field is by normalizing the detected signal to the actual received signal calculated using the geometry of the optics. One cause of this distortion is referred as the out-of-focus circle, which occurs when radiation from a target plane located at short or intermediate ranges is not focused onto the focal plane. A diffuse region of illumination, i.e., the blur circle caused by diffraction, is formed in the focal plane by far field radiation; however, a small detector positioned at that location cannot receive all of the near field radiation expected. The loss only occurs in the near field because far field backscattered radiation is focused by the receiver optics onto the detector (see Measures, 1984). The off-axis focus of the actual return signal changes at different locations due to re-alignment of the laser (see Jeness, 1997). An algorithm was developed that can calculate the telescope form factor experimentally and is calculated after movement to a new measurement location to avoid discrepancies due to re-alignment [Esposito, 1999]. This form factor is determined by calculating optical extinction in the clear atmosphere.

2.5 Extinction Measurement Technique

Extinction, given in units of km^{-1}, is the total attenuation of a laser beam through the atmosphere due to scattering and absorption by both aerosols and molecules [Measures, 1984]. The LAPS instrument measures extinction at three different

wavelengths using the gradients in molecular profiles [O'Brien, et. al., 1998; Li, et. al., 2000]. LAPS measures extinction using molecular profiles of Raman-shifted nitrogen at 607 nm resulting from the 532-nm transmitted wavelength and at 284 nm resulting from the 266-nm transmitted wavelength. Another extinction measurement is made by using the rotational Raman signal of nitrogen and oxygen at 530 nm from the 532 nm transmitted wavelength. The Beer-Lambert Law is used to calculate the extinction coefficient, α, using the measured signals, I, I_0, and the range bin size, x, and is given as [Measures, 1994, Stevens, 1996]:

$$\alpha = \frac{-\ln(I/I_0)}{2x} \quad . \qquad [2.2]$$

The total extinction in the atmosphere is given by the absorption and scattering of both molecules and aerosols and is shown in the following equation:

$$\alpha_{\text{tot}} = \alpha_{\text{mol,abs}} + \alpha_{\text{aer,abs}} + \alpha_{\text{mol,sca}} + \alpha_{\text{aer,sca}} \quad , \qquad [2.3]$$

where,

$\alpha_{\text{mol,abs}}$ is the extinction due to molecular absorption,
$\alpha_{\text{aer,abs}}$ is the extinction due to aerosol absorption,
$\alpha_{\text{mol,sca}}$ is the extinction due to molecular scattering,
$\alpha_{\text{aer,sca}}$ is the extinction due to aerosol scattering.

Extinction due to absorption by both molecules, $\alpha_{\text{mol,abs}}$, and aerosols, $\alpha_{\text{aer,abs}}$, at the 530-nm wavelength is negligible, since this wavelength is close to the transmitted wavelength, 532 nm, and the absorption at the visible wavelengths due to ozone is very small [Measures, 1984]. Extinction due to molecular scattering is easily estimated and that

signal is removed, resulting in profiles of extinction due to aerosol scattering. LAPS measures extinction at the three different wavelengths 284 nm, 530 nm, and 607 nm. Aerosol scattering optical extinction profiles at the visible wavelengths of 530 nm and 607 nm (see Figure 2.5) are very close in value to each other, but they are much less than the extinction values at the 284-nm channel because of the larger scattering cross-section of the small particles at this time. The extinction measurement at the ultraviolet wavelength, 284 nm, is also corrected for ozone absorption. Figure 2.5 shows a plot of the extinction due to aerosol scattering at each wavelength measured during the NE-OPS pilot study at a time when the atmosphere was relatively clean. Error bars are included to indicate the accuracy, and these will be discussed in detail in Section 2.13.

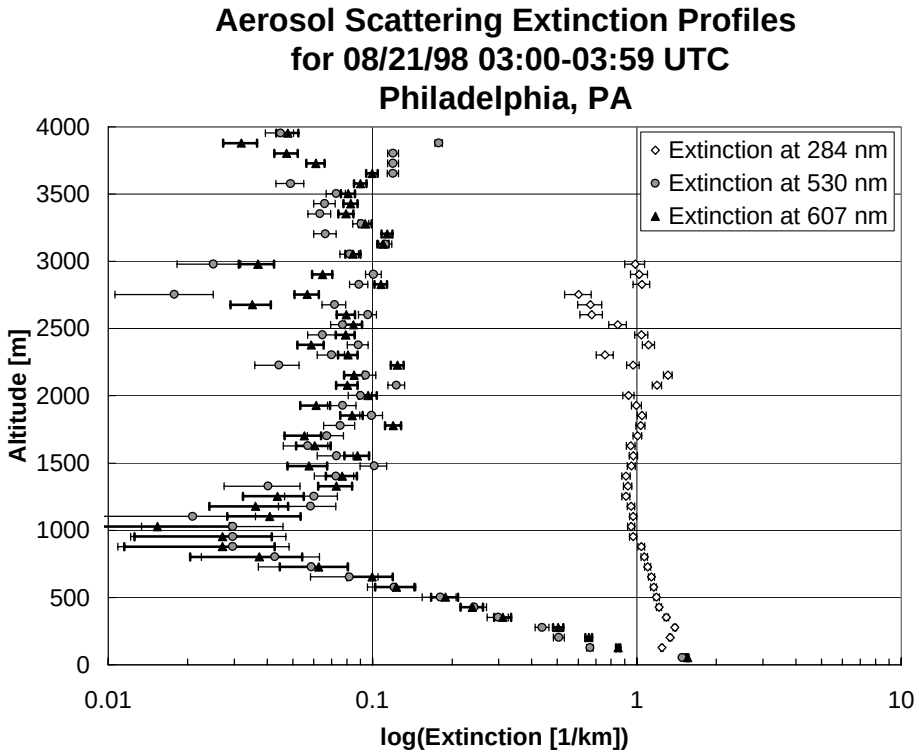

Figure 2.5. Vertical extinction profiles measured by LAPS at 284 nm, 530 nm, and 607 nm on 08/21/98 from 03:00–03:29 UTC show the error bars associated with the measurement at each altitude.

2.6 Telescope Form Factor Correction

The telescope form factor can be experimentally determined using data under very clear conditions that correspond to very low aerosol concentration. In extremely clear conditions, the extinction at 530 nm can be assumed to be due mostly to molecular scattering. Once the shape of the extinction curve below 800 m is determined during clear measurement conditions, it is possible to use a telescope form factor correction curve that is useful for calculations of extinction profiles at other times when aerosol scattering is present. The extinction due only to molecular absorption at ground level is found to be approximately equal to 0.015 km^{-1} at 530 nm [Measures, 1984]. Unfortunately, aerosols are usually present during the summer months on the East Coast, so these aerosols must be considered when determining a realistic value for extinction on a clear day at the measurement location. The error associated with the telescope form factor becomes less important as the aerosol extinction increases to values of 0.5 km^{-1} or larger. The relation of visibility to extinction was used to determine what the actual extinction would be on a clear day. The following equation for determining extinction was used [Measures, 1984]:

$$\alpha(\lambda_T) = \frac{3.91}{R_v}\left\{\frac{550}{\lambda_T}\right\}^q , \qquad [2.4]$$

where,

R_v is the meteorological visual range at which the transmission is 2%,
λ_T is the transmitted wavelength,
q is equal to 0.585 $R_v^{1/3}$.

For LAPS, the wavelength, λ, is set equal to the transmission wavelength of 532 nm, and the visual range, R_v, for a clear day on the East Coast is approximated to be 25 km. The

term q is then approximately 1.7. Using the relation in Equation 2.4, the extinction on a clear day in the East Coast is determined to be approximately 0.165, which is a factor of 10 higher than the value for extinction due purely to molecular absorption. This new value of extinction is used to fit the optical extinction measured, so that a form factor can then be determined from that fit. Once the form factor is determined, vertical profiles of extinction can be determined in the near field. Optical extinction profiles in the far field (800-5000 m) are directly calculated using the measured Raman signals. The signal is also range corrected by multiplying by the square of the range term to provide useful extinction profiles describing the aerosol content in the atmosphere.

2.7 Water Vapor Measurement Technique

Water vapor mixing ratio, also known as specific humidity, is measured at both ultraviolet and visible wavelengths. Ultraviolet channel measurements are made both day and night, while visible channel measurements are only made during the night. Daytime ultraviolet measurements are possible since they are made in the "solar blind" region of the ultraviolet spectrum (200-300 nm). The water vapor mixing ratio is determined by taking the ratio of the Raman signal for water vapor to the signal for molecular nitrogen, which represents a constant value of 78% of the atmospheric density [Esposito, 1999]. The water vapor mixing ratio is calculated by taking the ratio of the return signal at two different wavelengths, i.e., the 1st Stokes vibrational Raman shifted wavelengths of water over nitrogen, and multiplying by a calibration factor. The return signal of nitrogen (607 nm for visible channels, 284 nm for ultraviolet channels) is used to determine the density

of ambient air. The following equation is used to determine the vertical profiles of water vapor, W(z) [Esposito, 1999],

$$W(z) = K_{cal} \frac{S_{H2O}(z)}{S_{N2}(z)} \quad , \qquad [2.5]$$

where,

S_{H2O} is the received signal from the vibrational Raman shift of H_2O at 660 and 295 nm,
S_{N2} is the received signal from the vibrational Raman shift of N_2 at 607 and 284 nm,
K_{cal} is a calibration constant.

The calibration constant, K_{cal}, is found by fitting the ratio of S_{H2O} to S_{N2} to radiosonde data, or determined from the relative sensitivity of the two channels and the scattering cross-sections. Since the telescope form factor is not dependent on wavelength, it cancels out in this ratio and no correction for it is needed. However, the water vapor mixing ratios for both visible and ultraviolet channels must be corrected for molecular scattering [Esposito, 1999]. The correction for molecular scattering is applied from the $1/\lambda^4$ dependence on the extinction coefficient due to molecular scattering and applying it to ratio of the lidar signals. The wavelength dependence of aerosol scattering for the measured wavelengths is relatively much less sensitive than the molecular scattering, so it can be neglected in the ratio. By correcting for molecular scattering, Equation 2.5 becomes [Esposito, 1999]:

$$W(z) = K_{cal} \frac{S_{H2O}(z)}{S_{N2}(z)} \exp(\sigma_{H2O} - \sigma_{N2}) G(z), \qquad [2.6]$$

where,

σ_x is the is the Raman cross-section of x at the laser wavelength,
$G(z)$ is the difference in molecular scattering.

The term G(z) is derived using the standard atmosphere and can be obtained using the following relations [Esposito, 1999]:

$$G(z) = \int_0^z NH(z)\left[1 - \exp\left(\frac{z'}{H(z)}\right)\right]dz' \quad , \qquad [2.7]$$

$$H(z) = \frac{kT(z)}{mg} \quad , \qquad [2.8]$$

$$T(z) = T_0 + \gamma z \quad , \qquad [2.9]$$

where,

N	is the number density at ground level,
k	is Boltzman's constant,
m	is average mass per mole,
g	is gravitational acceleration,
T_0	is the surface temperature,
γ	is the lapse rate of –6.5 K/km.

The solar blind portion of the ultraviolet spectrum is also the region where ozone in the troposphere absorbs radiation, so the ultraviolet water vapor mixing ratio is corrected for ozone absorption. This correction is determined by taking the ratio of O_2 to N_2 and incorporating the extinction due to ozone. The water vapor ratio at ultraviolet wavelengths is given by [Esposito, 1999]:

$$W(z) = K_{cal} * \frac{S_{H2O}(z)}{S_{N2}(z)}\left(\frac{S_{O2}(z)}{S_{N2}(z)}\right)^{\frac{\sigma_{H2O}-\sigma_{N2}}{\sigma_{N2}-\sigma_{O2}}} \quad , \qquad [2.10]$$

where,

S_{O2} is the received signal from the vibrational Raman shift of O_2 at 277 nm.

2.8 Ozone Measurement Technique

The correction for ozone absorption in ultraviolet water vapor mixing ratio was expanded to develop a technique for measuring ozone using a Raman lidar. A DIAL (DIfferential Absorption Lidar) analysis of the Raman shifts of N_2 (284 nm) and O_2 (277 nm), which occur on the steep side of the Hartley absorption band of ozone, is used to obtain ozone measurements. The Hartley absorption band of ozone with the Raman wavelengths indicated can be seen in Figure 2.6.

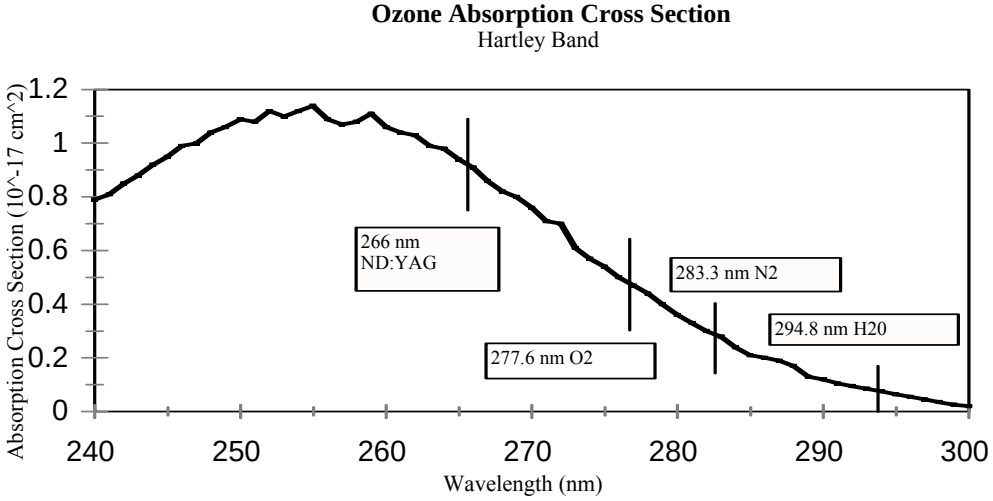

Figure 2.6. Hartley band absorption cross-section of ozone is shown with wavelengths associated with the lidar's 266-nm transmission and its associated Raman-shifted wavelengths used to measure ozone concentration [using data from Inn, et. al., 1953].

Vertical profiles of ozone are calculated by taking the ratio of the O_2 and N_2 Raman-shifted signals using the equation [Esposito, 1999]:

$$\frac{P_{O2}(z)}{P_{N2}(z)} = k_{system} * \exp\left[-\int_0^z [\alpha_m(\lambda_{O2}, z') - \alpha_m(\lambda_{N2}, z')]dz'\right] \exp\left[-\int_0^z [\alpha_{O3}(\lambda_{O2}, z') - \alpha_{O3}(\lambda_{N2}, z')]dz'\right], \quad [2.11]$$

where,

$\alpha_m(\lambda_x, z')$ is the attenuation due to molecular scattering at wavelength λ_x,
$\alpha_{O3}(\lambda_x, z')$ is the attenuation due to ozone absorption at wavelength λ_x,

k_{system} is a constant used for simplification, given by:

$$k_{system} = \frac{\xi_R(\lambda_{O2})}{\xi_R(\lambda_{N2})} \frac{\sigma_{O2}}{\sigma_{N2}} \frac{N_{O2}(z)}{N_{N2}(z)} \quad . \qquad [2.12]$$

This measurement must also be corrected for molecular scattering and absorption. The number density of ozone in a scattered volume is calculated by differentiating the integrated ozone number density, which has been corrected for molecular scattering and is given by the equation [Esposito, 1999]:

$$[O_3(z)] = \frac{d}{dz}\left[\ln\left(\frac{P_{O2}(z)}{P_{N2}(z)} \frac{1}{k_{system}} \right) \left(\frac{1}{(\sigma_{N2} - \sigma_{O2})} \right) + \frac{(\sigma_{O2} - \sigma_{N2})}{(\sigma_{N2} - \sigma_{O2})} G(z) \right]. \qquad [2.13]$$

Differentiating the integrated ozone density in Equation 2.13 provides the ozone concentration in parts per billion (ppb) at each altitude after the first range bin, so vertical profiles of ozone from the ground up were not available until now. The ozone concentration at the first range bin could not be calculated using Equation 2.13, since the integrated ozone density at the first altitude is the first term in the differentiation. The ozone concentration at the second range bin is determined by differentiating the integrated ozone densities between the third and first range bins and so on. This analysis placed the first measurement at approximately 113 m above ground level.

Extending the vertical profiles to the ground is desirable, so a new method was introduced for obtaining the vertical profiles of ozone starting at the ground. Ground-level measurements of ozone were measured during the NE-OPS 1998 campaign by the Philadelphia Air Management Association. These ground-level measurements were incorporated with the lidar ozone analysis, which permitted the determination of ozone

concentrations at the first range bin, and provided the measurement at the ground level. In order to accomplish this, the ground-level ozone must be included in the differentiation of the integrated ozone density. This allows the ozone concentration at the first range bin to be computed. The ground-level ozone concentration in ppb was converted to a form of integrated ozone density using a variation of Equation 2.13. The following relations were used to change ozone concentration into a form of integrated ozone density, denoted by IO_3:

$$IO_3 = \int_0^z O_3(z')dz' - \frac{\ln(k_{system})}{(\sigma_{N2} - \sigma_{O2})} - G(z) \quad , \qquad [2.14]$$

$$IO_3 = \frac{\ln\left(\frac{P_{O2}(z)}{P_{N2}(z)}\right)}{(\sigma_{N2} - \sigma_{O2})} \quad , \qquad [2.15]$$

In Equation 2.14, the range limits of the integral are determined according to the height of mean sea level, so the lower limit is the surface altitude of the location that the measurements were taken and the upper limit is 10 m above the surface altitude, so that the extinction due to ozone absorption at each meter can be determined. Since the ground-level ozone concentration was not measured by lidar, the term k_{system} could not be determined solely from Equation 2.12. Although the cross-sections and number densities of the molecules at the surface are obtainable, the efficiencies at the wavelengths are not applicable. However, the ratio of the efficiencies at each wavelength for lidar measurements is constant, so this value was used to calculate k_{system} at ground level. The difference in molecular scattering, G(z), associated with these wavelengths is so small in comparison with the ozone at these wavelengths that it can be neglected. By using the

ground-level integrated ozone density in the differentiation in Equation 2.13, the ozone concentration at the first range bin was calculated and the concentrations at higher altitudes were found to be shifted closer to the ground-level value. The error associated was incorporated into the procedure by using an average error for ground-level ozone.

This new technique that provides vertical profiles of ozone from the surface is valuable for determining the ozone concentration near the surface and for providing more accuracy to the lidar measurements. Figure 2.7 depicts vertical profiles of ozone measured at 15:00-15:59 UTC on 08/21/98, which shows fairly high levels of ozone. Figures 2.7 (a) shows vertical profiles of ozone without the ground-level measurement, and Figures 2.7 (b) shows vertical profiles of ozone from the surface. Note the shift in ozone concentrations in the first few range bins. This shift is a result of tying the ozone measurements to the ground-level measurement through differentiation.

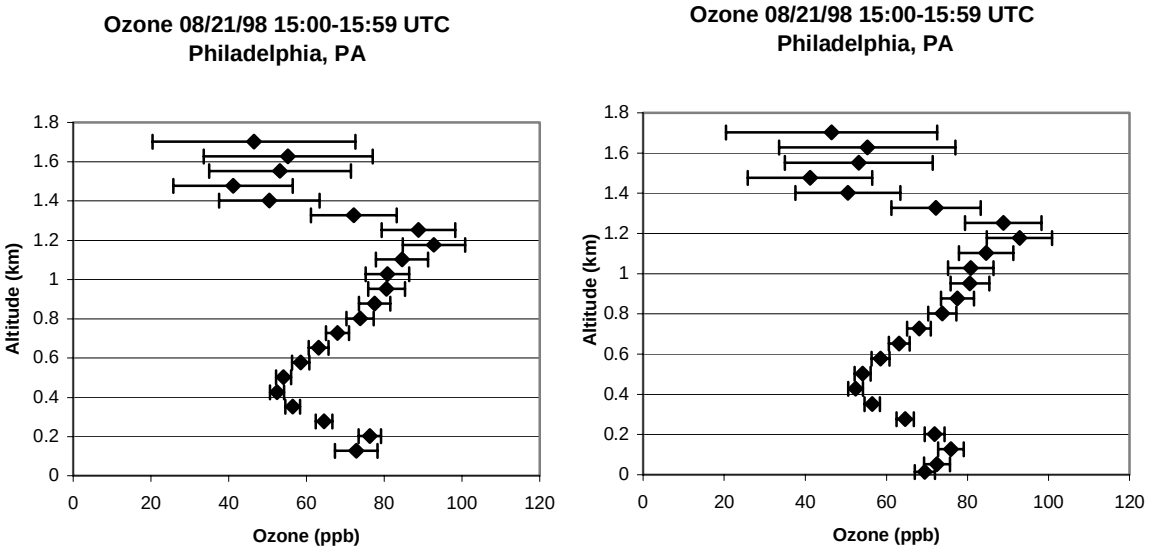

(a) (b)

Figure 2.7. Vertical profiles of ozone at 15:00-15:59 UTC on 8/21/98 measured in Philadelphia, PA shows (a) ozone without ground-level measurements; (b) lidar data integrated with ground-level measurements of ozone.

2.9 Temperature Measurement Technique

Temperature is measured by LAPS by taking the ratio at the two wavelengths of the rotational Raman scatter wavelengths of N_2 and O_2. The rotational Raman spectrum of these molecules is temperature dependent, and the thermal equilibrium distribution of their states can be represented by the distribution of the spectrum of Stokes and anti-Stokes rotational Raman transitions. The anti-Stokes spectrum is used so that any possible contribution from fluorescence is avoided. As temperature increases, the higher rotational states are populated, resulting in the lines further away from the transmitted wavelength being increased, while the lines closer to it decrease slightly. The Stokes and anti-Stokes rotational line intensities are depicted in Figure 2.8 [Haris, 1995].

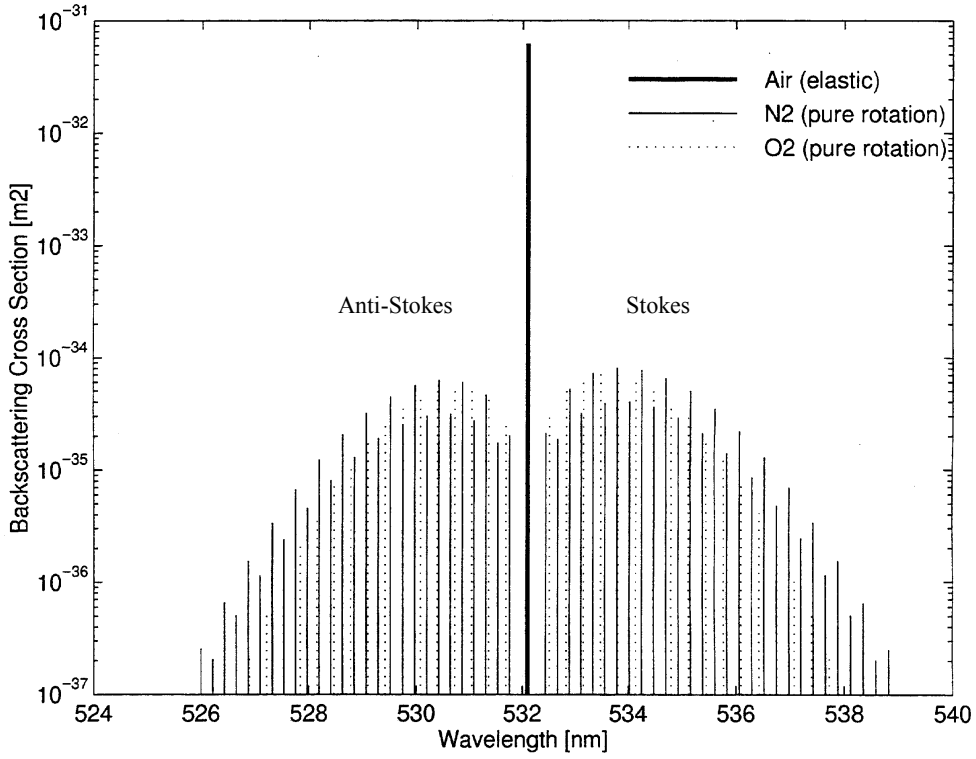

Figure 2.8. Stokes and anti-Stokes backscatter cross-sections for nitrogen and oxygen rotational line intensities for 532-nm scattered radiation [Haris, 1995].

The return signals at the visible wavelengths of 528 nm and 530 nm are used for the calculation of temperature. The ratio of these wavelengths is described in the following equation [Balsiger, et. al., 1996]:

$$R(T) = \frac{\sum_S \sum_J N_S \times A_S(J,T) X f_{530,S}(J)}{\sum_S \sum_J N_S \times A_S(J,T) X f_{528,S}(J)} = \frac{C_{530}}{C_{528}}, \quad [2.16]$$

where,

$R(T)$	is the lidar ratio as a function of temperature,
S	is the summation index over the molecular species,
J	is the summation index over the quantum numbers of the rotational states,
N_S	is the fraction of the species in the atmosphere,
$A_S(J,T)$	is the thermal population distribution of the rotational states,
$f_{530,S}$	is the filter transmission function of the 530-nm channel,
$f_{528,S}$	is the filter transmission function of the 528-nm channel
C_x	is measured signal at $\lambda = x$.

The ratio of the 530 nm and 528 nm signals must be fitted to radiosonde balloon data for calibration. The fit is performed using a least square method using the following equation:

$$T(R) = aR^2 + bR + c \quad , \quad [2.17]$$

where,

T(R)	is the temperature as a function of the lidar signal ratio,
R	is the lidar ratio of the 530-nm signal and the 528-nm signal,
a, b, and c	are calibration constants determined from filter sonde data.

These calibration constants are first set equal to constants determined by the sensitivities of the filters and then are calculated by adjusting the fit to the sonde data.

2.10 Backscatter Measurement Technique

Vertical profiles of backscatter from airborne particles are measured using a detector with a filter centered at the transmitted wavelength of 532 nm. The backscatter detector is a high-speed, high-resolution, photon-counting PMT that was added to the LAPS instrument in 1999. This PMT provides a resolution of 3 meters, which is much higher than the 75-meter resolution provided by the seven other PMT's. Backscatter from particles is determined using the backscatter lidar equation given in the following equation [Measures, 1984]:

$$\beta(\lambda_L, \lambda, R, r) = \sum_i N_i(R, r) \left\{ \frac{d\sigma(\lambda_L)}{d\Omega} \right\}_i^S L_i(\lambda) \Delta\lambda \quad , \qquad [2.18]$$

where

$N_i(R,r)$ is the number density of scatterer species i at range, R, and position, r,

$\left\{ \frac{d\sigma(\lambda_L)}{d\Omega} \right\}_i^S$ is the differential scattering cross section under irradiation with laser radiation at wavelength λ_L,

$L_i(\lambda)\,\Delta\lambda$ is the fraction of the scattered radiation that falls into the wavelength interval $(\lambda, \lambda + \Delta\lambda)$.

The backscatter of particles is closely related to extinction, and can in some simple cases be expressed in the following equation [Wiegner, 1998]:

$$\beta = B\sigma^k \quad , \qquad [2.19]$$

where,

B is a function of range

k is a constant

The actual relationship between extinction and backscatter is valuable because it can provide information on the changes in the particle size distribution. For a small particle size, the ratio of extinction to backscatter is constant. As particle size increases, the ratio increases as well.

Since the backscatter channel was not available in the LAPS instrument for the measurement campaign in 1998, the backscatter coefficient was measured using a Micro Pulse Lidar (MPL) Model 1000 prepared by Science and Engineering Services, Inc. This instrument will be described in the following section.

2.11 Micro Pulse Lidar Instrument

The Micro Pulse Lidar (MPL) Model 1000 is a compact, eye-safe lidar that measures backscatter using a high-repetition rate GaAlAs-diode laser-pumped Nd:YLF 2^{nd} harmonic at 523 nm to measure backscatter. It is capable of continuous, autonomous operation and provides data displaying the vertical distribution of particles/aerosols in the boundary layer [Lee, 1996; Hlavka, et. al., 1998; SESI, 1996]. The MPL consists of an optical transceiver, a scalar/controller unit, and a computer. A fiber-optic cable couples the optical output from the laser diode module located in the scalar/controller unit to the laser head located in the transceiver unit. The 523-nm transmitted wavelength is directed to the telescope through optical components. This out-going laser is fully expanded through the telescope for minimal beam divergence to spread the power over the full telescope aperture for the safety of operators [SESI, 1996]. The return signal is collected by a telescope and detected by a receiver unit. A polarizing beam splitter directs the green laser beam to the telescope and directs the backscattered 523-nm wavelength to the

photon counting detector. The MPL's detection system has one of the highest detection sensitivities in this class of instruments [SESI, 1996]. The pulse duration of green laser light is approximately 10 ns, and the photon counting detector generates TTL pulses of duration approximately 10 ns in proportion to the number of returning green photons. Data is collected in units of PhE/μS (TTL pulse counts/micro sec) [SESI, 1996]. The computer has a software package called WMPL that processes and displays the data in real-time as a signal proportional to the backscatter coefficient. Vertical profiles of the atmosphere and time-sequence plots are available. The system has fully overlapped optical alignment since the same telescope is used for transmitting and collecting; however, corrections to the raw data such as overlap, deadtime, afterpulse, and range correction, must be applied before aerosol analysis is performed [Lee, 1996, Hlavka, et. al., 1998; SESI, 1996]. These corrections were developed at NASA/GSFC, where the MPL was designed, by the MPL analysis team [Hlavka, et. al., 1998]. Table 2.3 shows the characteristics of the SESI Micro Pulse Lidar Model 1000 [SESI, 1996].

Table 2.3. Micro Pulse Lidar Model 1000 Optical Transceiver

Detection Range	60 km
Altitude Resolution	30, 75, 150, 300 m
Laser	Diode Pumped Nd:YLF
Wavelength	Single 523.5 nm
Output Pulse Energy	10 μJ
Pulse Repetition Rate	1 ~ 10 kHz
Pulse Duration	10 ns
Telescope Diameter (Cassegrain)	0.2 m
Field of View	< 50 μrad
Detector	Geiger Mode Avalanche Photodiode
Bandwidth	0.2 nm

2.12 Vignetting Correction

The return signals measured by LAPS need to be corrected for losses due to the atmosphere, such as absorption, and due to the instrument, such as the telescope form factor. Another loss of signal that must be accounted for is the vignetting that occurs in the optics of the LAPS unit. Vignetting is the shadowing of rays as they pass through an optical path [Hecht, 1990]. Due to this shadowing, signals from the near-field were being clipped, resulting in inaccurate data [Esposito, 1999].

The vignetting correction technique is accomplished experimentally. The effects of vignetting were noticed in both the ultraviolet and visible channels. Since the optical paths to each channel are different, the effects of vignetting for the channels are different, thereby, making the correction curves different. The return signal for a certain wavelength should remain unchanged if measured at the same wavelength simultaneously. If the wavelength of the filter is interchanged in the detector box, it can be assumed that any altitude changes in the ratio of signals at the same wavelength are due to vignetting. To obtain the ultraviolet vignetting correction curves, the 284-nm filter and the 295-nm filter are replaced by 277-nm filters, and the return signal is analyzed. The ratio of the return signals should be constant from the surface upward. First the ratio is normalized to one, and then any variation below 1 km is assumed to be due to vignetting [Esposito, 1999]. A multiplication curve is found that keeps the ratio constant and this is applied to the data. The same method is used for the visible channels, whereby a 530-nm filter is used for replacement of the visible filters. The vignetting correction improves the data in the lower altitudes for ozone, water vapor, and temperature.

2.13 Error Analysis

Error analysis involves determining the uncertainty of measurements and how these uncertainties affect calculations that are dependent upon those measurements. The uncertainty due to lack of precision in instruments can be expressed as the difference between the true or actual value and the measured value. Since the scattering cross-section and other parameters are known to accuracy of about 1-2 %, the major errors in the measurement are due to the photon counting statistics. If the uncertainty in the measurement is due to statistical fluctuations and not lack of precision, the uncertainties can be represented by the standard deviation, σ, of the measured quantity and are assumed to have a Poisson distribution [Bevington, 1969]. The Poisson distribution is applicable for measuring a large number of signals in a time interval, so it provides a good description for the lidar return of photon counts since the number of scattered photons returned is much smaller than the actual number scattered. Relative uncertainty is the ratio of the standard deviation to the average rate and can be expressed for a Poisson distribution as [Bevington, 1969]:

$$\frac{\mathrm{sd}}{\mathrm{x}} = \frac{\sqrt{\mu}}{\mathrm{x}} = \frac{1}{\sqrt{\mu}}, \qquad [2.20]$$

where,

sd is the standard deviation,
μ is the mean,
x is the number of events.

It is common in data analysis to use independent measurements as parameters for calculating dependent variables, which may be used for results. The uncertainty in these

independent variables must be carried through the calculations in order to define the uncertainty in the dependent variable, and this procedure is referred to as propagation of errors [Bevington, 1969]. The propagation of errors procedure can be applied to the lidar data when the ratio of signals is taken to calculate an atmospheric parameter, such as water vapor. The propagation of error of a ratio z=x/y is given by the following relation [Bevington, 1969; Esposito, 1999]:

$$\frac{sd_z}{z} = \sqrt{\left(\frac{sd_x^2}{x^2} + \frac{sd_y^2}{y^2} - 2\frac{r_{xy}\, sd_x\, sd_y}{xy} \right)}, \qquad [2.21]$$

where,

sd_z is the standard deviation of z,
sd_x is the standard deviation of x,
sd_y is the standard deviation of y,
r_{xy} is the correlation between x and y.

The correlation, r_{xy}, is neglected, since it is very small in comparison with the standard deviations. These statistical techniques are used to apply error bars to the measured signals, as shown in the extinction measurements in Figure 2.5.

Raman lidar techniques for measuring vertical profiles of the atmosphere have proven to be very useful in describing the dynamics of the atmosphere, as well as determining the distribution of chemical species and airborne particulate matter. Lidar profiles are also useful for atmospheric model evaluation, since vertical profiles provide information about the concentrations of PM and ozone in different layers of the atmosphere.

CHAPTER 3

Evolution and Relationship of Ozone and Particulate Matter

3.1 Ozone

Investigating the ozone concentrations in the lower atmosphere is essential for understanding pollution trends and aiding in pollution monitoring at the surface. Contributions to ozone formation in the lower atmosphere include the photochemical production from both local and distant chemical sources and downward transport from the stratosphere. Ozone is formed photochemically in both the stratosphere and in the lower surface layer of the troposphere, but its presence poses an environmental threat in the troposphere, and its absence in the stratosphere is a hazard. Ozone in the stratosphere occurs naturally and serves as a protective layer from ultraviolet radiation. The primary reaction mechanism that forms ozone in the stratosphere is the reaction of oxygen molecules with a free oxygen atoms [Arya, 1999]. The depletion of ozone in the stratosphere results in allowing more rays of harmful ultraviolet radiation to reach the Earth's surface. The depletion is tied closely to chlorofluorocarbons produced at the surface reacting in the stratosphere [Sillman, 1993]. The reactions that take place are a result of highly reactive chlorine and chlorine oxide reacting with the ozone molecules and oxygen and are shown below [Liou, 1980]:

$$Cl + O_3 \rightarrow ClO + O_2 \quad , \qquad [3.1]$$

$$ClO + O \rightarrow Cl + O_2 \quad . \qquad [3.2]$$

Emission controls have resulted in the reduction of the burden of the chlorofluorocarbons which catalytically remove ozone; however, this problem remains significant because the effects are long-term [Sillman, 1993].

Ozone pollution in the lower atmosphere is a serious problem and contributes to detrimental health issues. Ozone and its precursors are a key ingredient of urban smog, as well as major components of pollution in rural areas of the U.S. [Sillman, 1993]. Tropospheric ozone is photochemically formed from chemical emissions of nitrogen oxides and volatile organic compounds [Arya, 1999]. It is primarily produced in the polluted continental boundary layer since most of the nitrogen oxides (NO_x, NO_y) and reactive, volatile organic carbon compounds (VOC's) are emitted in that layer [Levy, et. al., 1997]. Amount of sunlight and temperature are key factors in the production of ozone. Ozone is produced only in the presence of sunlight, and ozone levels that exceed air quality standards primarily occur only when temperatures are above 25°C [Sillman, 1993]. When the temperature is high, ozone can also be formed from biogenic sources of VOC's, which are oils that are given off from leaves on certain types of trees. The main precursors of tropospheric ozone are caused by chemical emissions into the atmosphere from power plants, factories, and vehicles. These factors render urban areas as principal source locations for ozone production, but this does not exclude high levels of ozone from reaching rural areas. The large biogenic VOC emission in the Southeast U.S. is a principle source of the tropospheric ozone formation in that region, particularly when temperatures are above 30°C. Transport of ozone and its precursors is a strong contributor to high concentrations of ozone in outlying areas. Downward transport from the stratosphere also contributes to the ozone concentration in the troposphere [Levy, et.

al., 1997]. Ozone from the stratosphere is injected into the troposphere during the winter and spring at mid to high latitudes [Levy, et. al., 1997]. Although this contribution from the stratosphere is not large, it must be considered in ozone control strategies. More importantly, the production of ozone by reactions involving pollutants must be studied further, since production can be directly controlled.

The formation of ozone by nitrogen dioxide is a very significant anthropogenic source of ozone in photochemical smog and is described in the following equations [Finlayson-Pitts, et.al., 1993]:

$$NO_2 + h\nu\ (\lambda<430\ nm) \rightarrow NO + O \quad , \qquad [3.3]$$

$$O + O_2 + M \rightarrow O_3 + M \quad . \qquad [3.4]$$

The molecule NO_2 is photodissociated by sunlight to form a free oxygen atom. Ozone is formed when the free oxygen atom reacts with an oxygen molecule in the presence of a third molecule, M, which is needed for stabilization [Finlayson-Pitts, et.al., 1993]. The molecule NO can react with the ozone molecule to regenerate nitrogen dioxide, which may result in another cycle of ozone production. It may also react with organic molecules, such as HO_2, to form NO_2 without the destruction of ozone, which could result in an increase in the net concentration of ozone [Walcek, et.al., 1995]. These reactions are shown below:

$$NO + O_3 \rightarrow NO_2 + O_2 \quad , \qquad [3.5]$$

$$NO + HO_2 \rightarrow NO_2 + HO \quad . \qquad [3.6]$$

Reaction 3.5 is more dependent upon temperature than reaction 3.6 and increases production with increasing temperatures [Walcek, et. al., 1995]. The hydrogen oxide can also react with carbon monoxide, which has a longer life cycle, and produce HO_2 [Walcek, et. al., 1995]:

$$CO + HO \rightarrow CO_2 + HO_2 \quad . \qquad [3.7]$$

Increased amounts of HO_2 may cause increased amounts of NO_2, which leads to an increase in ozone as was shown in the preceding reactions. A termination point for these reactions can occur if nitrogen dioxide reacts with OH radicals and forms nitric acid [Finlayson-Pitts, et.al, 1993]:

$$OH + NO_2 \rightarrow HNO_3 \quad . \qquad [3.8]$$

Nitric acid is a harmful pollutant that may be formed along with ozone from pollutants emitted into the lower atmosphere and is also a key ingredient of acid rain [Finlayson-Pitts, et.al., 1993]. Another source of nitric acid that can be associated with ozone occurs at night. The nitrate radical NO_3 is formed in the presence of ozone and nitrogen dioxide and is described in the following reaction [Finlayson-Pitts, et.al., 1993]:

$$NO_2 + O_3 \rightarrow NO_3 + O_2 \quad . \qquad [3.9]$$

The nitrate radical that is formed can then react with another molecule of nitrogen dioxide to form nitrogen pentoxide, N_2O_5 [Finlayson-Pitts, et.al., 1993]. Nitric acid is formed by nitrogen pentoxide through hydrolysis on wet surfaces and is shown in the following reactions [Finlayson-Pitts, et.al., 1993]:

$$NO_3 + NO_2 \rightarrow N_2O_5 \quad , \qquad [3.10]$$

$$N_2O_5 + H_2O \rightarrow 2HNO_3 \quad . \qquad [3.11]$$

A description of ozone formation in the troposphere is shown in Figure 3.1 for a case where VOC's are absent and a case where VOC's are present [Arya, 1999].

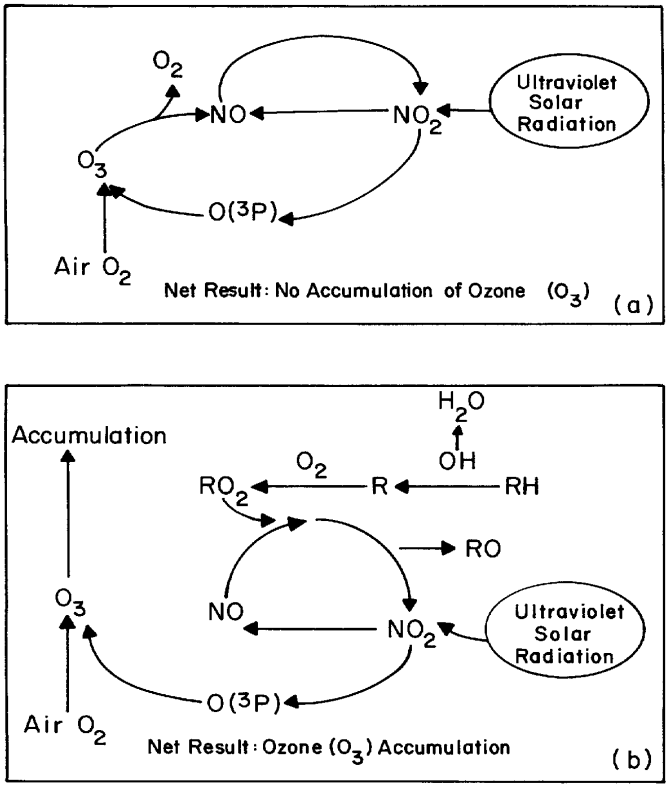

Figure 3.1. Tropospheric ozone formation: (a) in the absence of VOC's. (b) in the presence of VOC's [Arya, 1999].

Understanding the formation of ozone in the troposphere is important for determining what measures can be to be undertaken to control it. The above reactions demonstrate that ozone production is directly related to emissions of pollutants and may lead to the production of other chemical species, which could react and form additional pollutants. The transportation of both ozone and its precursors and the relationship of ozone with fine particulate matter will be explored in Section 3.3.

3.2 Fine Particulate Matter

Fine particulate matter is another important pollutant that affects air quality and has an impact on health. Fine particulate matter is distinguished by being smaller than 2.5 μm and is primarily formed by chemical processes that take place in the lower planetary boundary layer. Fine particles are primarily a result of combustion of fossil fuels from industry, power plants, automobiles, and residential heating systems [Albritton, et.al., 1998]. Figure 3.2 illustrates the particle size distribution, which indicates the categorization of fine and coarse particles [Albritton, et. al., 1998]. To be detected by lidar, the scattering cross-sections of the particles must be at least of the size corresponding to the accumulation mode. This mode is formed by growth of particles from the nuclei mode, which can occur through water coalescing on these particles or through conglomeration [Rogers, 1989]. Optical extinction measured by lidar corresponds to the amount and distribution of fine and coarse particles.

The major constituents that compose fine particulate matter (PM) in the U.S. are sulfur, nitrogen, and carbon [Hidy, et.al., 1998]. Fine particles can be transported long distances from where they were produced [Hidy, et.al, 1998]. Transportation of fine

particulate matter and its precursors can contribute significantly to the pollution levels on a regional scale, and the transport of precursors can be associated with the production of secondary particles in regions distant from the sources. The distribution and formation of fine particulate matter affects local and regional air quality.

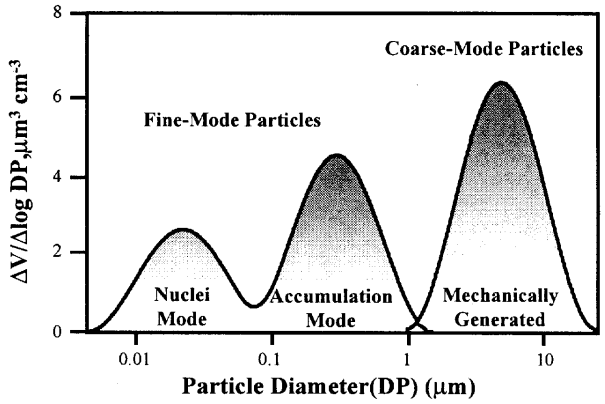

Figure 3.2. Volume size distribution of particulate matter [Albritton, et.al., 1998].

Determining the magnitude of the variation of pollutants on the lower atmosphere is essential when considering population exposure. The eastern part of the U.S. has significant visibility issues, and it has been recognized that enhanced aerosol particle concentrations occur with hazy conditions frequently occurring in eastern North America [Hidy, et.al., 1998]. The average visual range is about one-fifth of the visual range of what it would be without pollution [Albritton, et.al., 1998]. Current evidence strongly suggests that PM is a key factor in a range of health problems, if not directly causal [Mauderly, et.al., 1998]. Studies of an association between ambient particles and human health indicate that decreased emissions could lead to reductions in premature mortality and morbidity from cardiovascular and respiratory causes [Albritton, et.al., 1998]. The amount and length of exposure to PM determines the severity of adverse health effects. For example, long-term exposure to low concentrations may not lead directly illness or

death, but are directly associated with other adverse effects, such as respiratory and cardiovascular diseases, irritation of the eyes and throat, and impairment of athletic performance [Arya, 1999]. Monitoring and controlling the factors that contribute to the formation of fine particle matter are essential for lowering the risks associated with exposure to these pollutants.

The composition of aerosols is dependent upon how the chemicals in the atmosphere break down and react with each other. Within the air, aerosols grow and coagulate with each other, producing complex chemical mixtures [Kyle, 1991]. Toxic compounds can be formed from the dissociation of aerosols, and then can be transported great distances, thus having a great impact on the atmosphere in global proportions. Fine particles are typically sulfate, nitrate, ammonium ions, and carbon [Albritton, et.al., 1998]. Concentrations of aerosols tend to be higher in urban areas, when there are a number of local and regional sources, and during the summer months when suitable conditions exist for pollutant formation. Pollution episodes are characterized by exceptionally high concentrations of chemical species and particulate matter pollutants and can last for several hours to several days [Arya, 1999]. The formation of sulfates and nitrates is due to partially aqueous chemical oxidation. Sulfate formation involves H_2O_2, O_2, and O_3 reacting with dissolved SO_2 [Hidy, et.al., 1998]. Nitric acid is mainly formed through gas phase reactions between NO_2 and OH. Ammonium salts and sulfates can be formed through reactions with sulfuric acid and ammonia [Hidy, et.al., 1998]. Carbon is also a leading ingredient in ambient particle matter. Studies indicated that carbonaceous components could account for about 70% of fine particle matter mass in some urban areas [Hidy, et.al., 1998]. Understanding the formation of fine particulate matter is

important for establishing appropriate emissions controls to alleviate the poor atmospheric conditions.

3.3 Relationship of Ozone and Particulate Matter

Determining the relationship between ozone and fine particulate matter will provide an important tool for pollution control. Prior studies have shown that the concentrations of ozone and fine particle matter are related; however, the exact relationships are uncertain. The formation processes of both ozone and fine particle matter are chemically nonlinear, and it has been shown that high sulfate levels are associated with high ozone concentrations, but the reverse is not always true [Hidy, et.al., 1998]. A reduction in NO_x, that reduces the concentration of ozone, could also reduce the concentration of sulfates, since both O_3 and SO_2 are formed through oxidation processes. Reactions of NO_x and VOC photochemistry initiate ambient formation of secondary particulate matter and ozone [Hidy, et.al., 1998]. Figure 3.3 shows the chemical process pathways that link the formation of oxidants and secondary PM in the troposphere [Hidy, et.al., 1998]. Ozone and particulate matter are not only related through their formation processes, but also through chemical lifetime dependence and transportation.

The transport of particles and ozone is a substantial factor in addressing pollution issues. Transport processes can involve horizontal, i.e., front passages, or advection after vertical transport, i.e., convection [Kyle, 1991]. Vertical exchange processes and the spatial and temporal scales of atmospheric transport of fine particle matter and ozone are still under dispute [Philbrick, 1998]. Stable chemical species trapped above the boundary layer can be transported over great distances. Contributions to ozone levels at the surface

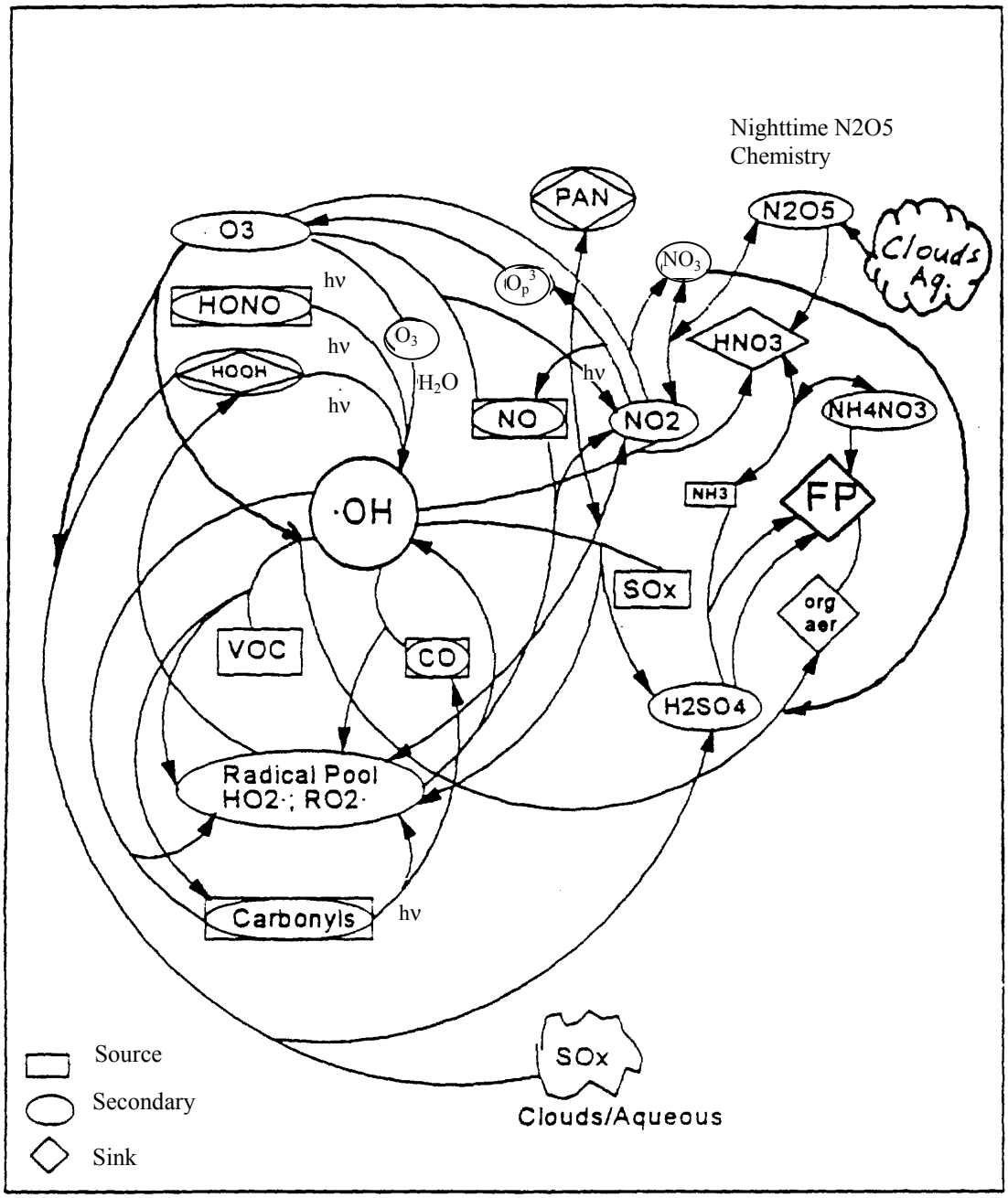

Figure 3.3. Tropospheric chemical process pathways that link oxidant and secondary particulate matter formation [Hidy, et.al., 1998].

can come from local sources, the direct transport of ozone and ozone precursors. Thermally dependent transport reservoirs of precursors remain stable in cool temperatures, but will dissociate when the temperature increases, thus releasing the precursors. Upon release, these precursors can react to readily form ozone and other pollutant species, increasing the levels of PM and ozone at the surface simultaneously.

One such transport reservoir is peroxyacetyl nitrate, commonly known as PAN. Peroxyacetyl nitrates are relatively stable at temperatures of the middle thermosphere and only become unstable in the high temperatures near the surface [Cardelino, et.al., 1990]. PAN primarily acts as a transport reservoir for reactive nitrates, which can then be released to form ozone when PAN decomposes in higher surface temperatures [Cardelino, et.al., 1990]. PAN was researched due to its stability and thermally dependent nature and was used as a hypothesis to explain the sudden increase in ozone at the surface during an air pollution episode on August 21, 1998. During this episode, an elevated plume descended and mixed with the rising convective boundary layer, resulting in a rapid increase in ozone and PM at the surface. Very little ozone was present inside the plume, so direct transport of ozone was not expected to be a contributor. The increase in ozone was so sudden that it was proposed that outside precursors were transported inside the plume, since local sources alone could not produce ozone that quickly. As the plume mixed into the boundary layer, the peroxyacetyl nitrates dissociated in the warmer temperatures at the surface. Investigating the origins and transport of pollutants will provide additional information to understand lower atmospheric air pollution episodes.

CHAPTER 4

Lidar Measurements of Atmospheric Properties

4.1 North-East Oxidant and Particle Study

The NARSTO-NE-OPS (North American Research Strategy for Tropospheric Ozone - North East - Oxidant and Particle Study) is a campaign dedicated to the investigation of the sources and chemical composition of atmospheric pollution episodes. The program includes the instruments that are most useful for describing the evolution of pollution events and examining the controlling factors of local meteorology on the particulate matter and chemical species distributions in the lower atmosphere. Local and regional factors are key in the development and dissipation of pollution events since they greatly influence the formation of both aerosol particles and ozone. Distinguishing between the local and regional sources that generate pollution episodes is important when considering emissions control regulations. The vertical and horizontal transport of pollutants, which is mainly controlled by meteorological trends, is essential in describing population exposure and risk. The NARSTO-NE-OPS research program's goals are to address these issues by providing measurements of atmospheric constituents that can be used for testing and development of atmospheric pollution models. The lidar technique has the capability of providing real-time vertical profiles and time-sequence plots of atmospheric properties. The lidar is most useful for investigating the vertical and horizontal structure of the atmosphere. The research effort benefits from the wide range of experiences that are based on the collaboration of a number of universities and agencies. The participants are shown in Table 4.1 [Philbrick, et.al., 2000].

Table 4.1 List of Investigators in the NARSTO-NE-OPS Program [Philbrick, et.al., 2000]

Penn State University Program management, lidar remote sensing, optical scattering, structure and dynamics
Millersville University Boundary layer meteorology, tethersonde measurements
Harvard University **School Public Health** Atmospheric gas and aerosol chemistry measurements and analysis, PM1, PM2.5, PM10, aerosol-size, EC/OC, sulfate, nitrate, toxics **Engineering and Applied Science** NO, NO_y measurements, Regional Reference Site at Harvard Forest
University of Maryland Instrumented small aircraft, UV flux and CO measurements, atmospheric chemistry
State University of New York Analysis and model calculations of polluted air masses
Rutgers University Environmental and Occupational Health Emissions inventories and chemistry modeling, particular experience in Phila. area
Brookhaven National Laboratory Highly instrumented DOE-G1 aircraft measurements of chemistry and aerosol properties
Philadelphia Air Management Services Laboratory Several measurement sites in Philadelphia, PAMS site
Drexel University Trace species measurements of filter samples using GC/MS and other techniques
Brigham Young University Measurement of particle volatile mass component and identification of volatile species
Pacific Northwest National Lab Rawinsondes at Philadelphia, RASS at West Chester, Ozonesondes at Phila. site
Argonne National Lab Rawinsondes, RASS, Sodar and Chemistry Laboratory at Centerton NJ
North Carolina A&T State University Remote sensing with lidar and sodar
North Carolina State University Laser remote sensing, particle optical properties measurements

4.2 Description of Lidar Data

The lidar data presented here were taken during the NE-OPS pilot study of August 1998 and comparisons were made with data taken by other instruments. Vertical profiles of optical extinction, water vapor, and ozone were taken by the Penn State LAPS instrument, and the backscatter measurements were made by the SESI Micro Pulse Lidar.

Lidar measurements are very worthwhile because they provide remotely measured profiles of atmospheric constituents, as well as a picture of the dynamics of the atmosphere. Time sequence plots of these vertical profiles provide a description the horizontal and vertical structures of the atmosphere during a period of time. Both the LAPS and MPL instruments take data in one minute intervals. The LAPS lidar data provides useful results for water vapor and extinction with 1-5 minute integration and a minimum of 30-minute integration for ozone and temperature. The time sequence data presented here is 30-minute integration and 5-minute time steps, so that features have some smoothing. The MPL data uses one-minute steps.

The sequence of plots shown in the following sections depict an air pollution episode, that occurred on 20-22 August 1998 in Philadelphia, PA, which exhibited increases in both ozone and aerosol levels. During this period, an aloft plume was mixed downward by the rising convective boundary layer, which produced sudden large increases in backscatter, extinction, and ozone. The ozone levels increased so rapidly that local sources are probably not the sole contributors. The ozone was not directly transported as evidenced by the lack of ozone present in the plume. Therefore, it has been hypothesized that the plume contained a transport reservoir of ozone precursors that was mixed to the surface, then dissociated and released these precursors, which were then available to freely react and form ozone. A likely transport reservoir is PAN, which is relatively stable at the cool temperatures of the middle troposphere, but decomposes rapidly in the warmer temperatures at the surface. PAN thermally dissociates into NO_x, which is a primary precursor of ozone. The rate of thermal decomposition of PAN from one important reaction, which forms H_3CCOO_2 and NO_2, is given by the following

empirical relation, where T is temperature in Kelvin [Beine, et.al., 1986; Finlayson-Pitts, et. al., 1986; Atkinson, et. al., 1984]:

$$\text{Rate} = 1.95\text{x}10^{16}e^{(-13{,}543/T)}\ [s^{-1}] \qquad [4.1]$$

This relation serves as a basis for a general description of the thermal dissociation of PAN, but it ignores the reformation of PAN [Beine, et. al., 1986; Finlayson-Pitts, et. al., 1986; Atkinson, et. al., 1984]. Figure 4.1 shows the rate of PAN thermal decomposition using a vertical profile of temperature measured by LAPS on 21 August 1998 at 04:20 - 04:50 UTC, which is a time period before the plume mixed with the rising boundary. As temperatures increase, the rate of PAN decomposition increases rapidly. The rapid increase would occur in the warmer temperatures at the lower altitudes (below 1500 m), as shown in Figure 4.1.

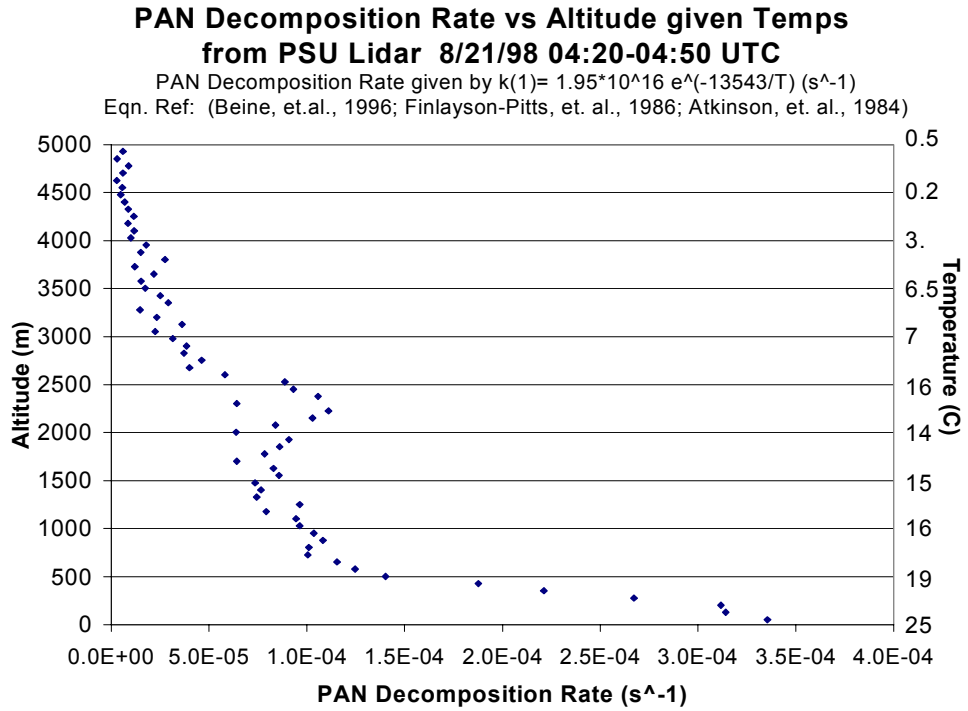

Figure 4.1. PAN thermal decomposition rate as a function of temperature at altitudes corresponding to temperatures measured by LAPS on 21 Aug 1998 04:20-04:50 UTC shows PAN decomposition rate increases quickly with increasing temperatures if an air mass is transported to the surface [based on Atkinson, et. al., 1984].

The temperature profile measured during the early morning of 21 August 1998 was used to determine the decomposition rate of PAN, which is significantly larger between the surface and 500 meters. The time sequence plots in Figures 4.2, 4.3, 4.5, and 4.7 begin at 09:00 UTC (05:00 local time), which is just before sunrise and ends at 19:00 UTC (15:00 local time). The sequence includes the build up of convective activity during the morning hours and concludes about two hours after the plume and convective boundary layer combine. This episode has been used to investigate conditions for meteorological control of the ground level concentrations and population exposure to ozone and particulate matter.

4.2.1 Backscatter

The measurements of backscatter provide information about the aerosol content in the atmosphere. Figure 4.2 shows parts of the aloft plume mixing downward and the increase of backscatter when an aloft plume mixed downward into the rising convective planetary boundary layer. The mixing occurred around 17:00 UTC (1 PM local time), which is when the boundary layer should be close to reaching its maximum height. Part of the plume mixing downward can be seen at around 1.5 to 2 km at approximately 16:30 UTC (450 min). The backscatter measurement is given in units of PhE/μsec, or TTL pulse counts per second and is range-corrected. This signal is proportional to the backscatter coefficient and provides high spatial resolution of the distribution of particulate matter. Backscatter measurements can be used in conjunction with the Raman extinction profiles to describe variations of the airborne aerosol particulate matter.

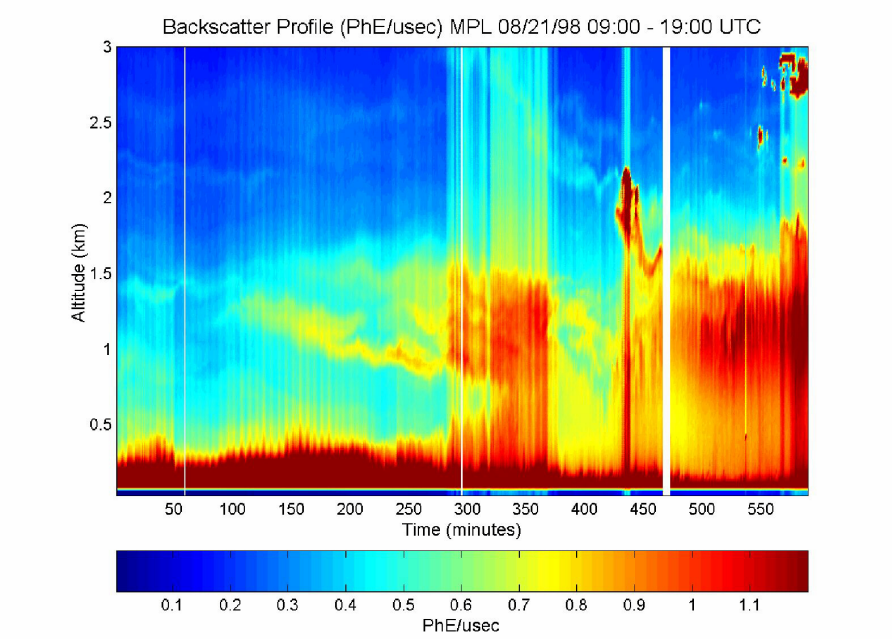

Figure 4.2. MPL time sequence backscatter profiles on 08/21/98 09:00-19:00 UTC shows downward motion of the plume which mixes with the rising boundary layer, and the following increase at approximately 18:00 UTC (540 min).

4.2.2 Extinction

An understanding of the characteristics and distribution of airborne particulate matter (PM) during periods of atmospheric pollution events can be established through analysis of extinction profiles. Extinction increases when the laser beam propagates through specific media, such as water vapor or aerosols, as scattering from these particles affects extinction [Mulik, 2000]. Figure 4.3 shows the LAPS extinction measurement during the August 1998 pollution episode. A distinct increase in extinction can be seen when the downward-moving plume mixes with the rising boundary layer. This increase is important because it indicates that the particle size and/or density is increased, which is most likely due to conglomeration of particles reacting with each other to form secondary particles in the lower atmosphere. The plume itself cannot be seen in Figure 4.3, since

the particles, if present, in the plume must be so small that they do not contribute to the optical extinction at 284 nm. The LAPS data is clipped at a set error, so that the data displayed does not show artificial features due to processing. The white area in the plot are due to signal with large error or missing data. The decrease in the height of the profiles is probably just due tp the loss of laser power by scattering at lower altitudes. The plume was located at approximately 2.5-3 km at 09:00 UTC and at 1.5 km during the mixing at 18:00 UTC.

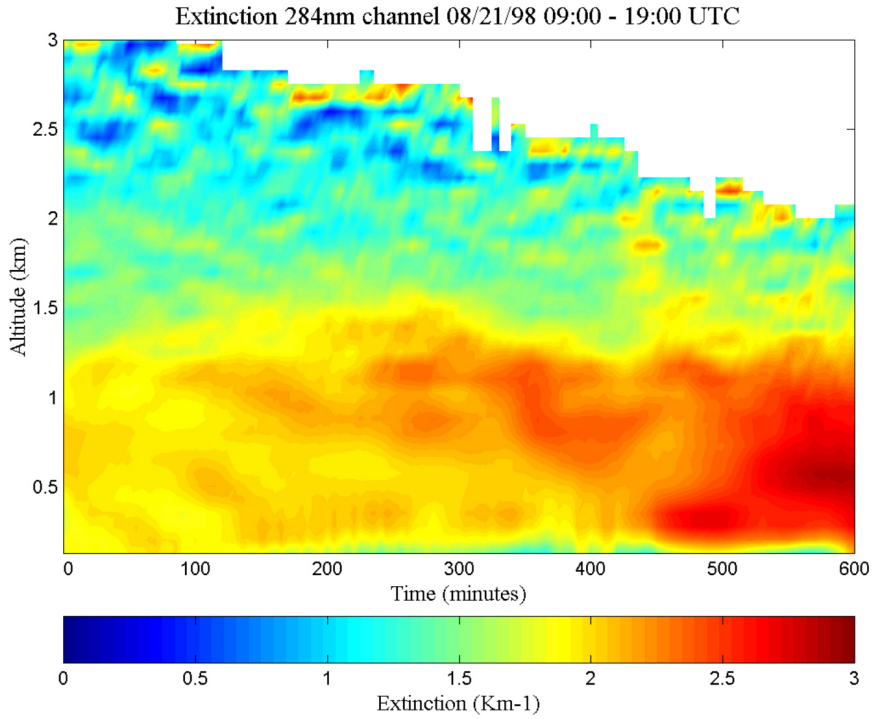

Figure 4.3. LAPS time sequence extinction profiles on 08/21/98 09:00-19:00 UTC shows the increase of extinction when the plume mixes with the rising boundary layer.

The plots in Figure 4.4 depict vertical profiles of extinction at 284 nm integrated for thirty minutes during two different periods with their corresponding error bars. Figure 4.4 (a) shows a vertical profile of extinction from 10:00 to 10:29 UTC on 21

August 1998. Figure 4.4 (b) shows a vertical profile of extinction from 18:00 to 18:30 UTC on 21 August 1998.

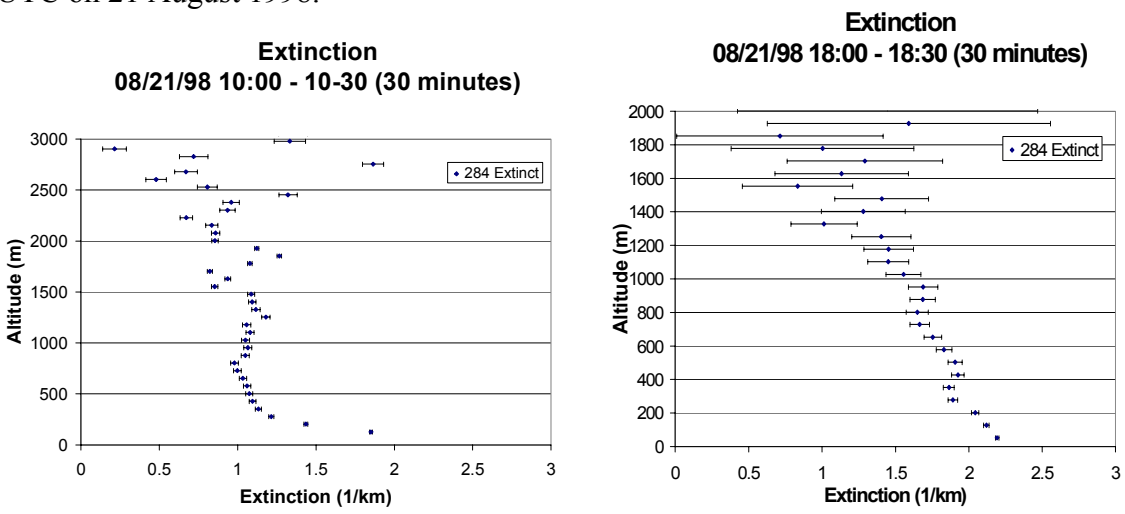

(a) (b)

Figure 4.4. Vertical profiles of extinction with error bars for measurements on 8/21/98; (a) at 10:00-10:29 UTC before the pollution event occurred. (b) at 18:00-18:30 UTC an increase in extinction occurs as the mixing of the plume and boundary layer began.

Extinction measurement analyses, in coordination with water vapor, backscatter, and ozone measurements, aid in understanding the causes of reduced visibility and pollution.

4.2.3 Water Vapor Mixing Ratio

Water vapor profiles provide a continuous monitor of the height of the planetary boundary layer and information about short-term dynamical processes in the planetary boundary layer. Vertical profiles of water vapor mixing ratio also serve as a tracer for transport of atmospheric constituents. Figure 4.5 shows the time sequence vertical profile water vapor mixing ratio during the pollution event in August 1998. A clear portrait of the aloft air mass can be seen moving in time, as it descends from approximately 2.5 km to 1 km during 10 hours. The plume is located at around 2.5-3 km at 09:00 UTC and has a water vapor mixing ratio concentration of approximately 8 g/kg with patches of higher

concentrations. As the plume descends to about 1.2 km at around 17:00 UTC (480 min), the water vapor mixing ratio increases to 15 g/kg. The rising convective boundary layer from sunrise to mid-afternoon is also evident in the plot. The height of the convective boundary layer increases from a few hundred meters to approximately 1.2 km and the water vapor concentration is increased from 12:00 (8 AM local-180 min) – 17:00 UTC (480 min). The exact timing of mixing downward of the overhead plume and boundary layer, which occurred at approximately 17:00 UTC (480 min), is also shown in Figure 4.5. The turbulence of the mixing is also displayed by the variations in the plot during that time. The plume could have contained ozone precursors that were rapidly mixed to the surface by the convective activity in the PBL and then thermally dissociated to produce ozone and other pollutants.

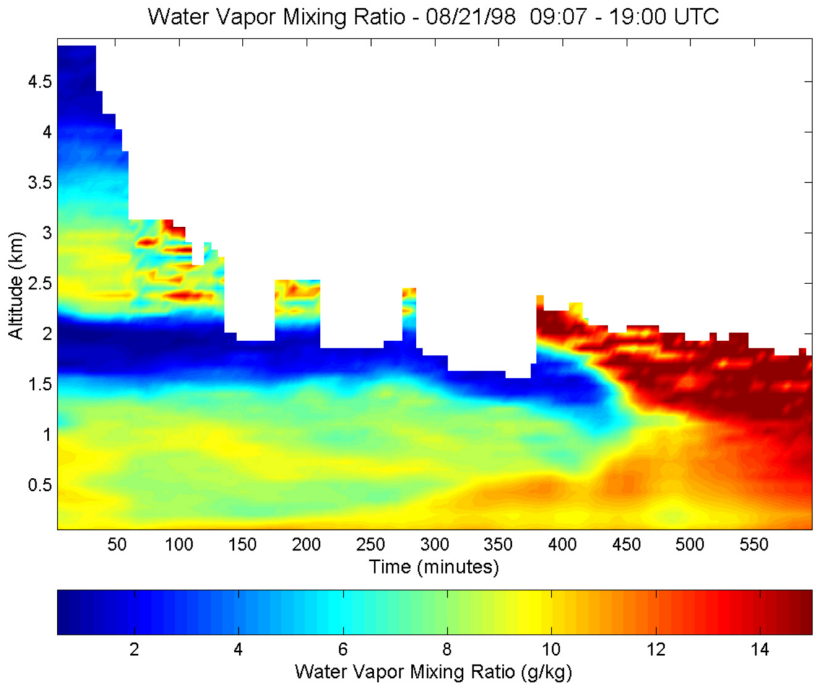

Figure 4.5. LAPS time sequence water vapor profiles on 08/21/98 09:00-19:00 UTC depicts the aloft plume descending and mixing with the rising convective BL.

The pollutants contained in the plume could have been transported great distances before reaching the surface. The water vapor time sequence plots provide information on when the plume reached the area and how long it traveled before mixing downward. The meteorology during the mixing would explain the reasons for the mixing, and the content of the plume would account for the sudden increases in backscatter, extinction, and ozone at the surface.

Vertical profiles of water vapor integrated for thirty minutes are shown in Figure 4.6. Figure 4.6 (a) depicts a profile of water vapor with its associated error bars on 21 August 1998 from 10:00 to 10:29 UTC, when the plume was aloft at around 2.5 km. Figure 4.6 (b) shows the vertical profile of water vapor 21 August 1998 from 17:00 to 17:29 UTC, when the plume is starting to mix down into the boundary layer. Water vapor profiles provide a tracer of the boundary layer dynamics, which is important in describing the distribution of ozone and particulate matter in the lower atmosphere.

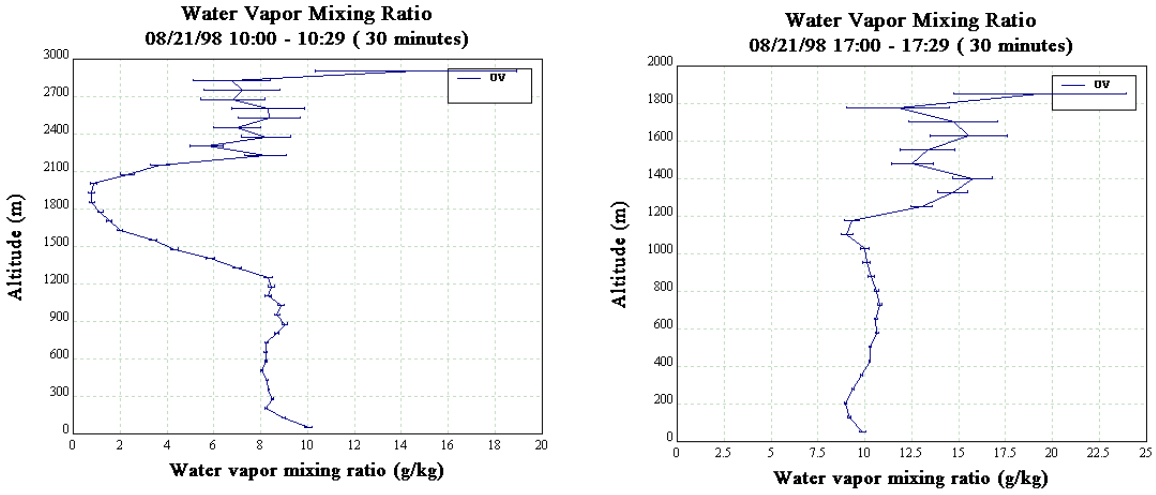

(a) (b)

Figure 4.6. Vertical profiles of water vapor with error bars for measurements on 8/21/98; (a) at 10:00-10:29 UTC with the plume located around 2.5 km, (b) at 17:00-17:29 UTC just as the plume is starting to mix with the boundary layer.

4.2.4 Ozone

The time sequence plot of ozone shown in Figure 4.7 indicates a sudden increase in ozone concentration during the mixing of the aloft air mass with the rising boundary layer. The ozone concentration increased from 70 ppb to 120 ppb in approximately 3 hours from approximately 15:00 UTC to 18:00 UTC. There is not much ozone located in the plume itself, as indicated in the Figure 4.7. It is hypothesized that the plume transported ozone precursors in a thermally dependent reservoir, which dissociated in the warmer temperatures at the surface during the mixing and released precursors, which quickly produced the ozone observed from rapid chemical processes. It is hypothesized that the transport reservoir was peroxyacetyl nitrate (see Figure 4.1), which has these characteristics and dissociates into ozone precursors with a very rapid rate temperatures above 30°C. It would be unlikely that local sources would be able to produce ozone that quickly. There is an indication that nuclei mode particles were brought into the region which resulted in the sudden rise of ozone, since the ozone and PM concentrations increased when the boundary layer had risen to the height of the plume [Zhang, 1999]. The boundary layer's height increased, while the aloft plume moved downward due to circulation around the high-pressure cell located over the southeast to allow for fumigation, or a mixing downward, to occur [Mulik, 2000]. Figure 4.3 shows a simultaneous increase of particulate matter just before the ozone event occurred. The speed of onset of ozone is consistent with the transport of ozone precursors by the plume that resulted in a multi-day high regional ozone in the eastern Mid-Atlantic [Ryan, 1999]. During the mixing, the ozone increased dramatically from 70 ppb to 120 ppb. The ozone

profile does not indicate high levels of ozone in the elevated plume, so the direct transport of ozone is improbable.

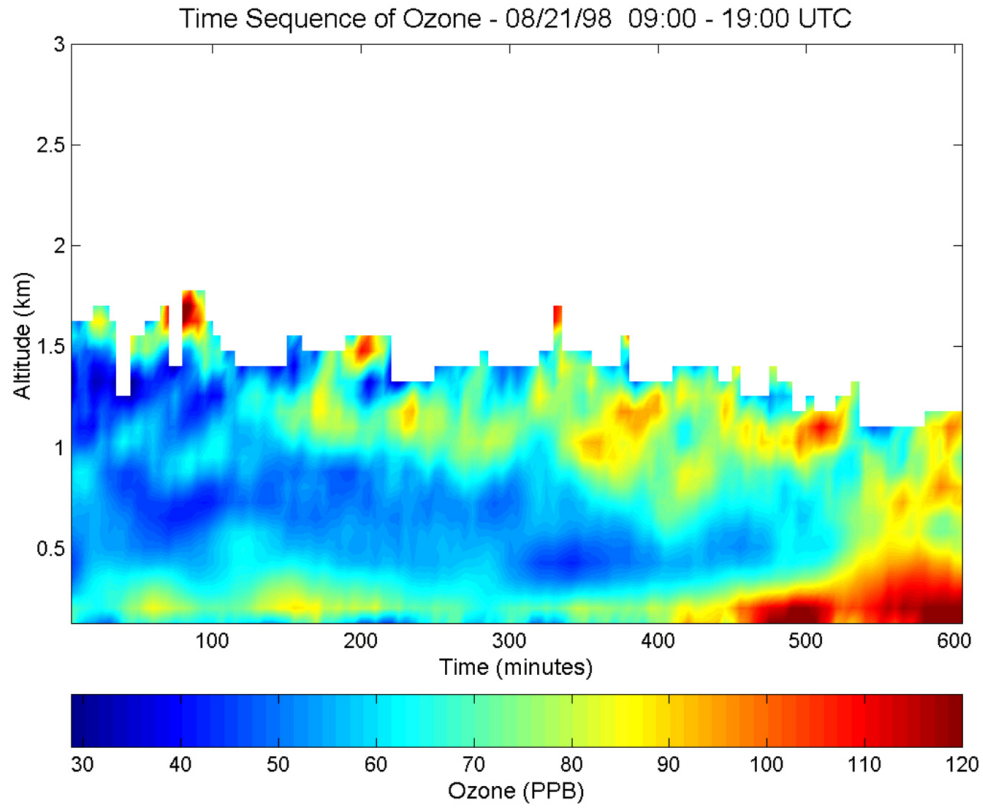

Figure 4.7. LAPS time sequence ozone profiles on 08/21/98 from 09:00-19:00 UTC displays the rapid increase of ozone at around 17:00 UTC (480 min) when the plume mixed with the rising convective boundary layer.

Vertical profiles with error bars of ozone integrated for one hour at each altitude are displayed in Figure 4.8. Figure 4.8 (a) shows a vertical profile of ozone on 21 August 1998 from 10:00 to 10:59 UTC before the pollution event occurred. A noticeable increase of ozone in shown in Figure 4.8 (b), which displays the vertical ozone near 17:00 UTC on 21 August 1998, just as the downward mixing of plume occurred.

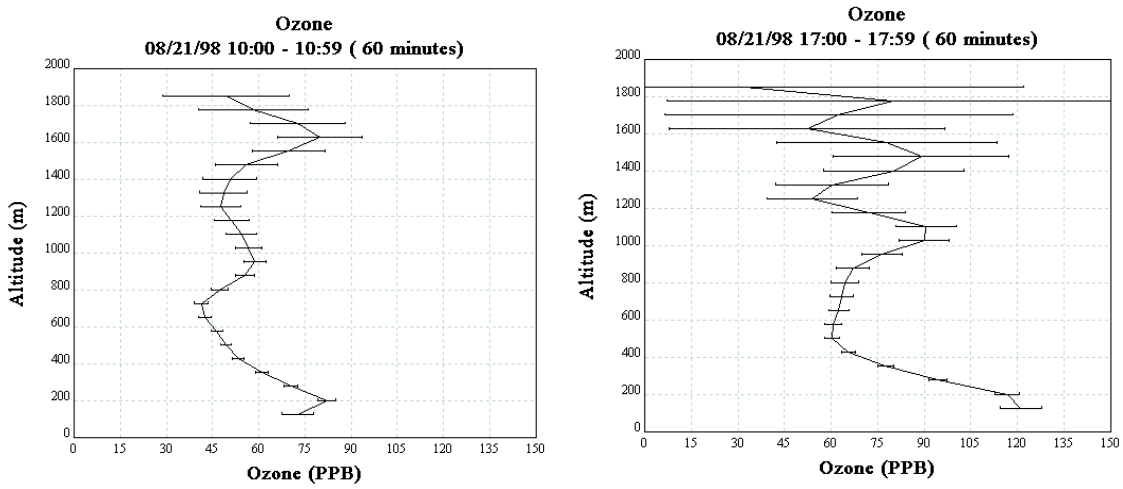

(a) (b)

Figure 4.8. Vertical profiles of ozone with error bars for measurements on 8/21/98; (a) at 10:00-10:59 UTC when the surface ozone was around 70 ppb (b) at 17:00-17:59 UTC just as the plume mixes with the BL with ozone levels around 120 ppb.

4.3 Comparisons

Several comparisons with other instruments can be made to aid in verification of the data. The backscatter and extinction measurements performed by the MPL and LAPS were compared. Figure 4.9 shows a MPL backscatter time-sequence profile on 19 August 1998 from 14:00 UTC to 16:59 UTC. There is a layer of particulate matter located around 1.5 km, which was observed by the backscatter measurement being at approximately 3 PhE/μs. Figure 4.10 shows a time sequence of extinction measured by LAPS during the same time period, and the same layer of particulate matter was measured. The layer of scattering observed in the visible backscatter and ultraviolet extinction occurs near the top of the PBL. At this location, the highest relative humidity occurs and is associated with condensation growth of aerosol size, and the larger particles increase optical scattering in the region. Differences in these measurements are seen in

the bottom portion of the plots, where the backscatter is high and the extinction is low. This is most likely due to the difference in the transmitted wavelengths and the correction factors applied to the data in the near field. The streaking seen in the MPL backscatter plot is due to the instrument resolution.

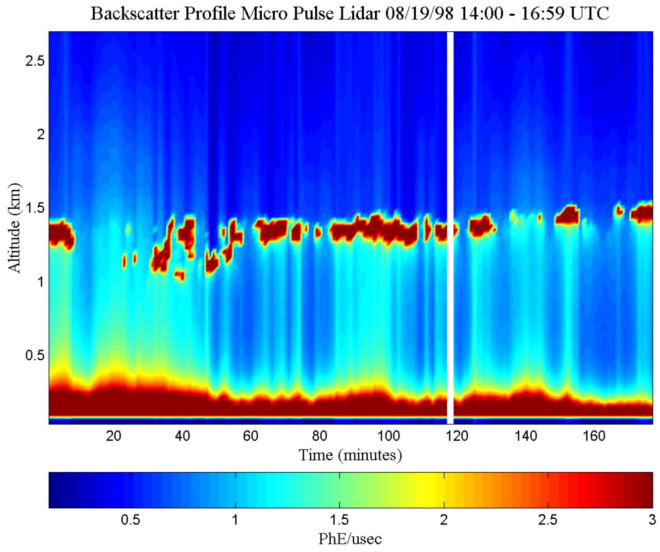

Figure 4.9. MPL time sequence backscatter profiles on 08/19/98 14:00-16:59 UTC shows a layer of particulate matter located at 1.5 km.

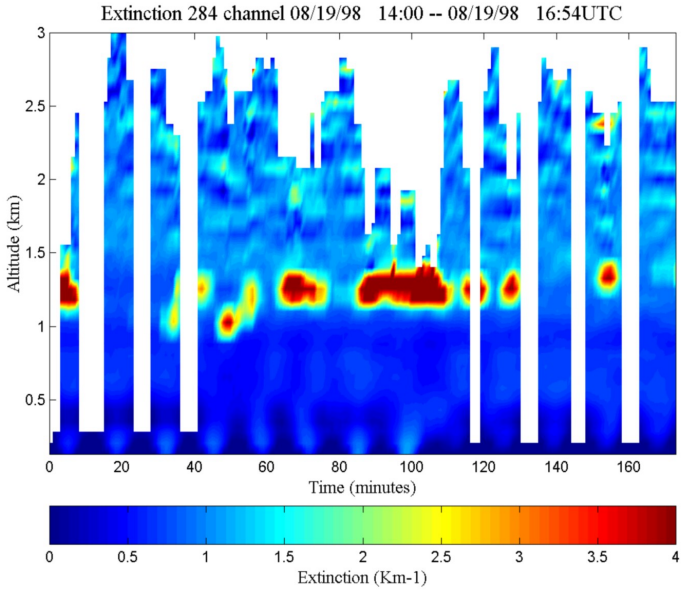

Figure 4.10. LAPS time sequence extinction profiles on 08/19/98 14:00-16:59 UTC shows the same layer of particulate matter at 1.5 km measured by the MPL.

Several of the same features occur in both sets of measurements; notice the features between 65 and 75 minutes and between 85 and 105 minutes. When the features are examined, the visible backscatter shows a thinner layer at a slightly higher altitude. The fact that the ultraviolet extinction is wider and extends to lower altitude is probably due to the wider distribution of the smaller particles that scatter the ultraviolet radiation, and possibly some effect of the larger altitude range bins. The visible backscatter would occur near the top of the PBL because the larger particles scattering visible radiation would be found at the peak in relative humidity.

Figure 4.11 depicts a time sequence of vertical ozone profiles on 20 August 1998 from 02:30 – 03:30 UTC and shows a layer of ozone at around 1.8 km.

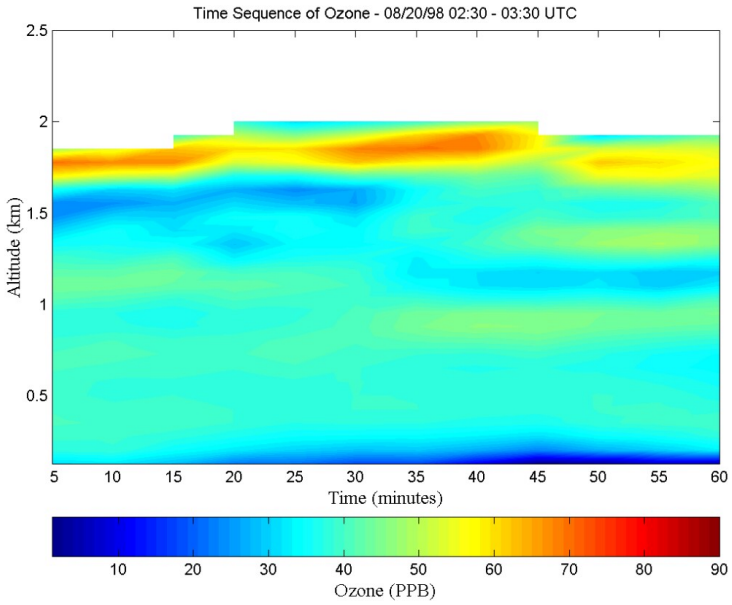

Figure 4.11. LAPS time sequence ozone profiles on 08/20/98 from 02:30-03:30 UTC displays a thin layer of ozone at 1.8 km.

A comparison of data during the same period was performed with the University of Maryland's aircraft [Doddridge, 2000]. This comparison is made for integrated ozone on

20 August 1998 from 02:45 to 03:35 UTC and is shown in Figure 4.12. From the plot in Figure 4.12, it can be seen that the measurements compare well at the lower altitudes. The error at the higher altitudes is a result of higher error in the lidar measurements, since the return signal is weaker and due to the lidar being stationary, whereas the aircraft is in motion.

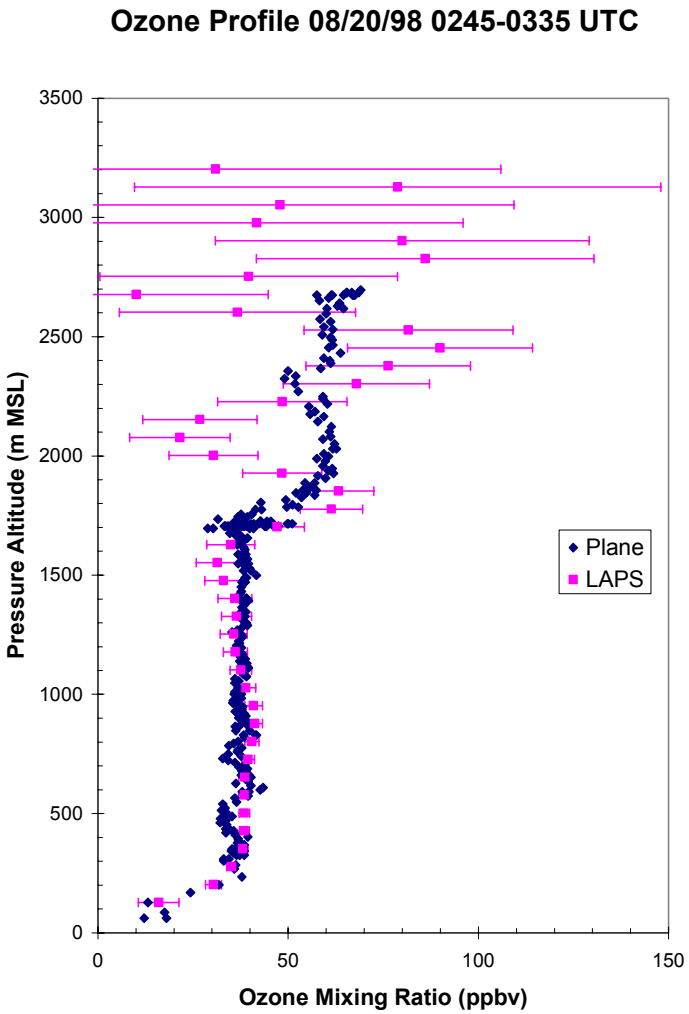

Figure 4.12. Vertical profiles of ozone measured by the PSU LAPS instrument the University of Maryland aircraft show good correlation (Aircraft data provided by Dr. B. Doddridge, University of Maryland).

Comparison was made using water vapor mixing ratio, or specific humidity, data on 20 August 1998 from 18:30 to 18:40 UTC from Penn State's lidar, University of Maryland's aircraft, and Millersville University's Tethersonde and is shown in Figure 4.13 [Doddridge, 2000; Clark, 2000]. The ground point measured by a sensor on top of the LAPS unit is also plotted. The height of the boundary layer is shown around 1500 meters.

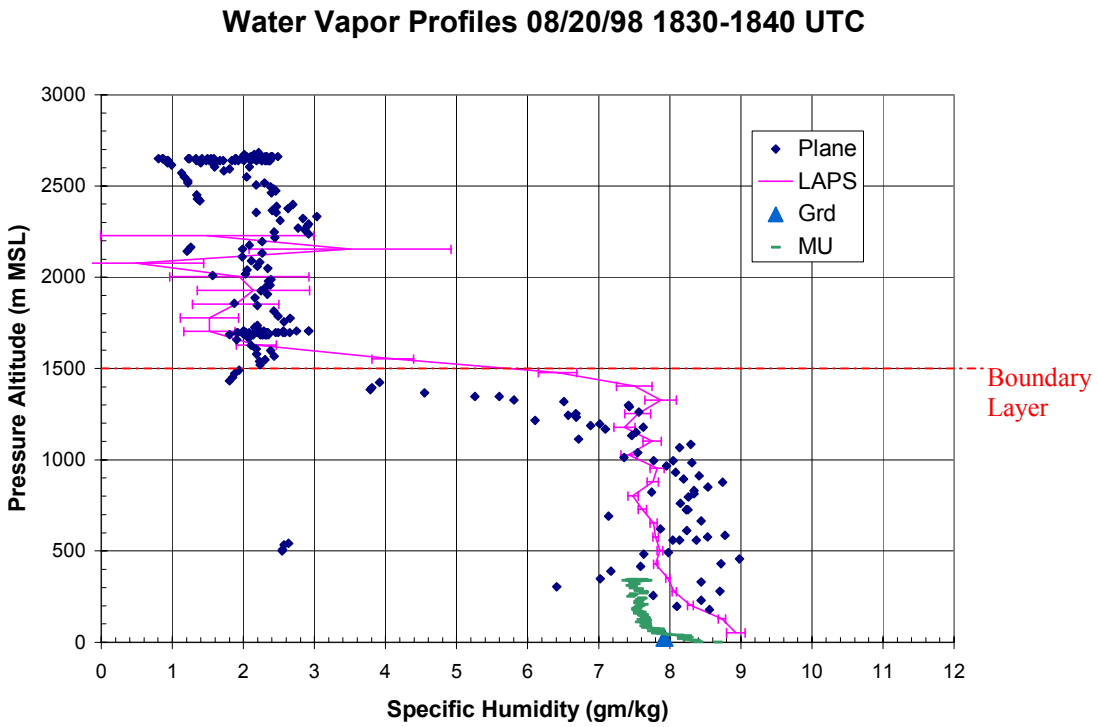

Figure 4.13. Vertical profiles of water vapor mixing ratio measured by the PSU LAPS instrument, instruments on the University of Maryland aircraft, instruments on the Millersville University tethersonde, and the ground point sensor show good correlation (Aircraft data provided by Dr. B. Doddridge, University of Maryland, and tethersonde data provided by Dr. R. Clark, Millersville University).

Comparisons with other instruments are helpful not only for verification purposes, but also for understanding and analyzing pollution events. The pollution episode that occurred on 21 August 1998 in Philadelphia, PA was also observed by ground-level

measurements. Figure 4.14 shows the ground-level ozone and $PM_{2.5}$ measurements from 09:00 to 19:00 UTC on 21 August 1998. The ground-level ozone data was provided by Philadelphia Air Management Services, and the $PM_{2.5}$ measurements were provided by the Harvard School of Public Health. Ground-level ozone increase from approximately 10 ppb to 100 ppb, and ground-level $PM_{2.5}$ increased from approximately 15 to 30 $\mu g/m^3$ over the 10 hour period. The increases in both ground-level ozone and $PM_{2.5}$ occurred at around 18:00 UTC, which is when the plume mixed with the boundary layer. The ground-level measurements provide a verification of the lidar vertical profiles of the backscatter, extinction, and ozone, while the lidar vertical water vapor profiles provide information on mixing and transport.

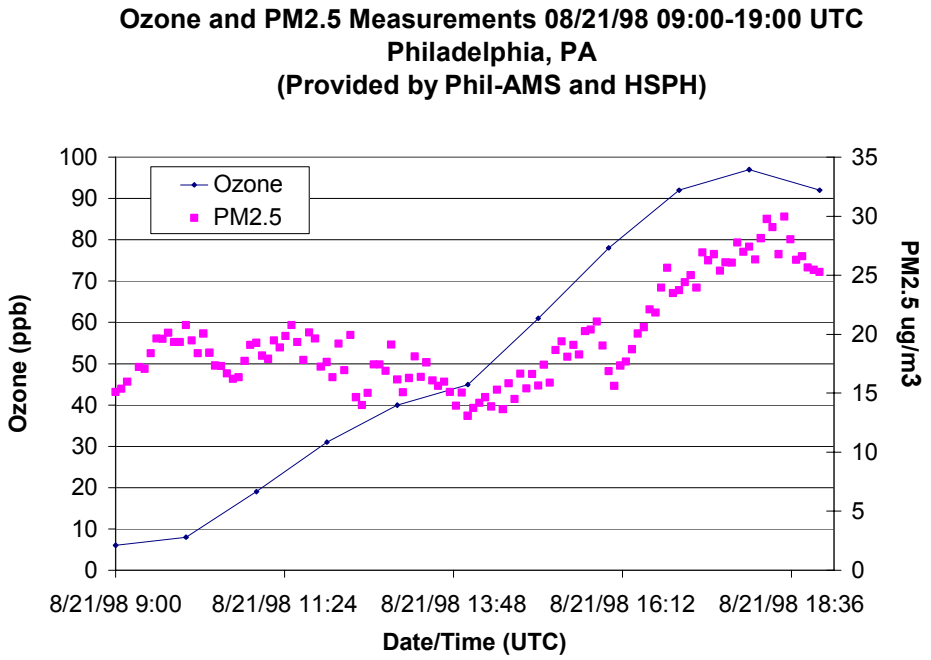

Figure 4.14. Ground-level ozone and $PM_{2.5}$ measurements on 08/21/98 from 09:00-19:00 UTC show simultaneous increases, when the plume mixed with the rising convective boundary layer (Ozone data provided by W. Miller, Phil-AMS, and $PM_{2.5}$ data provided by G. Allen, HSPH).

Comparisons with measurements from the 1999 NE-OPS campaign were made to determine how unique the rapid rise of ozone during the 21 August 1998 pollution episode was. Measurements were made during the 1999 NE-OPS campaign during a two-month period at the same location in Philadelphia, PA. Eight pollution episodes were observed during the 1999 campaign. Figure 4.15 shows a time-sequence plot of ozone measured by LAPS and depicts the start of an ozone event that occurred on 3-4 July 1999. Although, the ozone concentration reached a higher level than on 21 August 1998, there was a steady increase of ozone, which increased only about 30 ppb in 2 hours.

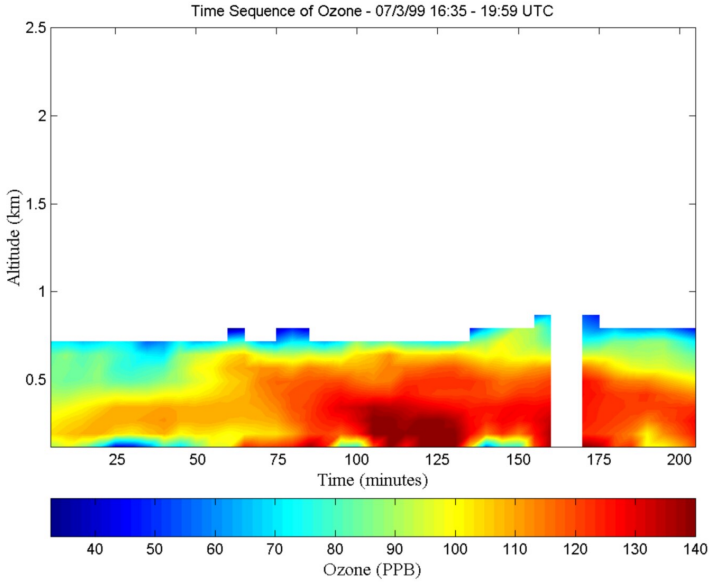

Figure 4.15. LAPS time sequence ozone profile on 07/03/99 from 16:35-19:59 UTC displays a steady increase of ozone.

The measurements obtained during the NE-OPS pilot study have provided valuable data on the evolution of pollution events that exhibit increases in both ozone and particulate matter.

CHAPTER 5

Conclusions

The investigations into pollution episodes in the northeastern U.S. conducted during the NARSTO-NE-OPS 1998 pilot study yielded important findings that can aid in the understanding of the evolution and dissipation of pollution events. The study was performed in an urban environment, where local discharge of pollutants, as well as transport from distant sources, have strong contributions to the concentrations of the primary pollutants that produce ozone and fine particulate matter. Ozone and fine particulate matter are directly related to existing air pollution problems at the surface, such as declining visibility and adverse health effects. Ozone is photochemically formed in the troposphere by volatile organic compounds and nitrogen oxides and is stable enough to be transported large distances in elevated plumes. Ozone precursors can also be transported as stable chemical species, which can be released by thermal dissociation to form ozone near the surface. Fine particulate matter is made up of particles smaller than 2.5 μm, such as sulfates, nitrates, and carbon-based molecules. Ozone and its precursors can be transported large distances, and these contribute to ground-level pollution concentrations on a regional scale. Transport reservoirs can remain stable and travel for great distances in the cool temperatures of the middle troposphere and then before being dissociated in warm surface temperatures, thus releasing pollutant precursors, which can rapidly react and form particulate matter and ozone.

Lidar techniques were utilized to explore the characteristics of the pollution episodes and their sources. Lidar is a remote sensing technique that probes the

atmosphere by transmitting a laser pulse of energy and measuring the backscatter from photons. Profiles of backscatter, extinction, water vapor, and ozone were measured using two different lidar systems, the PSU Raman lidar, LAPS, and the SESI Micro Pulse Lidar. The LAPS instrument transmits a laser at two wavelengths, 532 nm and 266 nm, and measures the scattered photons at Raman shifted wavelengths associated with the vibrational and rotational energy states of O_2, N_2, and H_2O. The Micro Pulse lidar transmits a laser at 523 nm and measures the backscatter at the same wavelength. The backscatter and extinction measurements provide information on particulate matter concentrations and their vertical distribution in the lower atmosphere. The water vapor measurements provide a tracer for boundary layer dynamics. Time sequences of these profiles yield information of the vertical and horizontal structure of the atmosphere during a period of time. The ozone measurements provide a constant monitor of concentrations of this pollutant from the surface to three kilometers. These measurements help describe the dynamical processes that occur in the lower atmosphere, especially during pollution episodes and have shown the importance of vertical mixing, horizontal transport, and storage of precursor materials.

An interesting pollution event that was observed on 21 August 1998 in northeastern Philadelphia, PA, during the NE-OPS pilot study was examined. This pollution episode depicted an aloft plume mixing with the rising boundary layer near 1.2 km, which resulted in sudden increases in both ozone and aerosol levels. The resulting pollution episode produced ozone values reaching 120 ppb, and PM values of 30 $\mu g/m^3$. It is hypothesized that ozone precursors were transported into the region by the plume and then vertically mixed to the surface by normal convective activity. At the high

surface temperatures, thermal dissociation of the precursor reservoir resulted in rapid increase of ozone. An ozone precursor transport reservoir that could have been a source of the rapid ozone production was peroxyacetyl nitrate (PAN) because it would be stable during transport at mid-troposphere temperatures and would decompose in higher temperatures at the surface. The PAN decomposition rate increased by a factor of 4 from temperatures at around 15°C at 2 km to temperatures at 25°C at the surface around 200 m. The lidar data taken during this episode illustrated the importance of studying the transport of pollutants and their effects. The lidar measurements were compared with aircraft and tethersonde measurements taken by University of Maryland and Millersville University, respectively. These comparisons showed good correlation and provided additional information used for analyzing the pollution episode.

References

Albritton, Daniel L., and Daniel S. Greenbaum, "Atmospheric Observations: Helping Build the Scientific Basis for Decisions Related to Airborne Particle Matter," Proceedings of the PM Measurements Research Workshop, Chapel Hill, North Carolina, July 22-23, 1998.

Arya, S. Pal, Air Pollution Meteorology and Dispersion, Oxford University Press: Oxford, 1999.

Atkinson, R. and A.C. Lloyd, "Evaluation of Kinetic and Mechanistic Data for Modeling of Photochemical Smog," J. Phys. Chem. Ref. Data, 13, 315, 1984.

Balsiger, Franz, Paul T. Haris, and C. Russell Philbrick, "Lower Tropospheric Temperature Measurements Using a Rotational Raman Lidar," Optical Instruments for Weather Forecasting, SPIE Vol. 2832, Denver, CO, pp.53 – 60, Aug. 1996.

Beine, Harald J., Daniel A. Jaffe, Donald R. Blake, Elliot Atlas, and Joyce Harris, "Measurements of PAN, Alkyl Nitrates, Ozone, and Hydrocarbons During Spring in Interior Alaska," J. of Geophysical Res., Vol. 101, No. D7, May 1996, p. 12,613-12,619.

Berman, Stephen, Jia-Yeong Ku, and S. Trivikrama Rao, "Spatial and Temporal Variation in the Mixing Depth over the Northeastern United States during the Summer of 1995," Journal of Applied Meteorology, 1999.

Bevington, Philip R. and D. Keith Robinson, Data Reduction and Analysis for the Physical Sciences, WCB/McGraw-Hill, Boston, 1969. pp. 38-52.

Burle Industries, Inc., Photomultiplier Handbook, 1980.

Cardelino, C.A., and W.L. Chameides, "Natural Hydrocarbons, Urbanization, and Urban Ozone," J. of Geophysical Res., Vol. 95, No. D9, August 1990, p. 13,971-13,979.

Clark, R.D., "Measurements of PM2.5, O3, and Meteorological Variables Obtained Using Tethered Balloons During the NARSTO-NE-OPS Pilot Study," Proceedings of the A&WMA Specialty Conference and Exhibition, PM2000: Particulate Matter and Health, Charleston, South Carolina, pp. 4AS3: 6-7, January 24-28, 2000.

Doddridge, B.G., "An Airborne Study of Chemistry and Fine Particles Over the U.S. Mid-Atlantic Region," Proceedings of the A&WMA Specialty Conference and Exhibition, PM2000: Particulate Matter and Health, Charleston, South Carolina, pp. 4AS2: 4-5, January 24-28, 2000.

Durbin, William, "Lidar Measurements of Ozone in the Lower Atmosphere," Master of Science Thesis for Penn State University, Department of Electrical Engineering, December, 1997.

Esposito, Steven T., "Applications and Analysis of Raman Lidar Techniques for Measurements of Ozone and Water Vapor in the Troposphere," Master of Science Thesis for Penn State University, Department of Electrical Engineering, May, 1999.

Esposito, Steven T. and C. Russell Philbrick, "Raman/DIAL Technique for Ozone Measurements," Proceedings of the Nineteenth International Laser Radar Conference, NASA Langley Research Center, Hampton, VA, NASA Conf. Publ. 207671, pp. 407 - 410, July 1998.

Finlayson-Pitts, B.J., and J.N. Pitts, Jr., Atmospheric Chemistry, John-Wiley, New York, 1986.

Finlayson-Pitts, B.J. and J.N. Pitts, Jr., "Atmospheric Chemistry of Tropospheric Ozone Formation: Scientific and Regulatory Implications," Journal of Air & Waste Mgmt., Vol. 43, pp. 1091-1099, August 1993.

Haris, P.A.T., "Pure Rotational Raman Lidar for Temperature Measurements in the Lower Troposphere," Ph.D. Dissertation, The Pennsylvania State University, 1995.

Hecht, E., Hecht Optics Second Edition, Boston, MA: Addison-Wesley Publishing Co., 1990.

Hidy, G.M., Philip M. Roth, J.M. Hales, and Richard Scheffe, "Oxidant Pollutants and Fine Particles: Issues and Needs," Journal of Air and Waste Management, June 1998.

Hlavka, Dennis L., James D. Spinhirne, and James R. Campbell, "Aerosol Analysis Techniques and Results from Micro Pulse Lidar," Proceedings of the Nineteenth International Laser Radar Conference, NASA Langley Research Center, Hampton, VA, NASA Conf. Publ. 207671, pp. 155-163, July 1998.

Inn, Edward C., and Yoshio Tanaka, "Absorption Coefficient of Ozone in the Ultraviolet and Visible Regions," Journal of the Optical Society of America, Vol. 43, No. 10, Oct. 1953, pp. 870-873.

Jeness, J.R., D.B. Lysak, Jr., and C.R. Philbrick, "Design of a Lidar Receiver with Fiber-Optic Output," Applied Optics Vol. 36, No. 18, pp. 4278 – 4284, 1997.

Kyle, Thomas G, Atmospheric Transmission: Emission and Scattering, Pergamon Press: Oxford, 1991.

Lee, H.S., I.H. Hwang, J.D. Spinhirne, and V.S. Scott, "Micro Pulse Lidar for Aerosol and Cloud Measurement," Selected Papers of the 18th International Laser Radar Conference (ILRC), pp. 7-10, Berlin, 22-26 July 1996.

Levy II, H., P.S. Kasibhatla, W.J. Moxim, A.A. Klonecki, A.I. Hirsch, S.J. Oltsman, and W.L. Chameides, "The Global Impact of Human Activity on Tropospheric Ozone," Geophysical Research Letter, Vol. 24, No. 7, Pages 791-794, April 1, 1997.

Li, G., G.S. Chadha, K.R. Mulik, and C.R. Philbrick, "Characterization of Properties of Airborne Particulate Matter from Optical Scattering Using Lidar," Proceedings of the A&WMA Specialty Conference and Exhibition, PM2000: Particulate Matter and Health, Charleston, South Carolina, January 24-28, 2000, pp. 4ASP1: 8-10.

Liou, K.N., An Introduction to Atmospheric Radiation, California: Academic Press Inc., 1980.

Mauderly, Joe, Lucas Neas, and Richard Schlesinger, "PM Monitoring Needs Related to Health Effects," Proceedings of the PM Measurements Research Workshop, Chapel Hill, North Carolina, July 22-23, 1998.

Measures, Raymond M., Laser Remote Sensing.Wiley-Interscience, New York: 1984.

Mulik, K.R., G. Li, G.S. Chadha, and C.R. Philbrick, "Evolution of Air Pollution Events Determined from Raman Lidar," Proceedings of the A&WMA Specialty Conference and Exhibition, PM2000: Particulate Matter and Health, Charleston, South Carolina, pp. 4ASP2: 11-13, January 24-28, 2000.

O'Brien, M.D., T.D. Stevens, and C.R. Philbrick, "Optical Extinction from Raman Lidar Measurements," Optical Instruments for Weather Forecasting, SPIE Proceedings Vol. 2832, pp. 45-52, 1996.

Philbrick, C.R., "Raman Lidar Measurements of Atmospheric Properties," Atmospheric Propagation and Remote Sensing III, SPIE Vol. 2222, 922-931, 1994.

Philbrick, C. Russell, "Investigations of Factors Determining the Occurrence of Ozone and Fine Particles in Northeastern USA," Measurement of Toxic and Related Air Pollutants - Proceedings of a Specialty Conference Cosponsored by the Air and Waste Management Association and the U.S. EPA's National Exposure Research

Lab, Volume 1, pp. 248-260, 1998.

Philbrick, C. Russell, "Raman Lidar Capability to Measure Tropospheric Properties," Proceedings of the Nineteenth International Laser Radar Conference, NASA Langley Research Center, Hampton, VA, NASA Conf. Publ. 207671, pp. 289-292, July 1998.

Philbrick, C.R., R.D. Clark, P. Koutrakis, B.G. Doddridge, W.C. Miller, S.T. Rao, P. Georgopolous, L. Newman, "Investigations of Ozone and Particulate Matter Air Pollution in the Northeast (NE-OPS 98)," Proceedings of the A&WMA Specialty Conference and Exhibition, PM2000: Particulate Matter and Health, Charleston, South Carolina, pp. 4AS1: 1-3, January 24-28, 2000.

Rogers, R.R., and M.K. Yau, A Short Course in Cloud Physics , Pergamon Press, Oxford, Chapter 6, pp. 81-98, 1989.

Ryan, William, Ozone Forecast and Technical Discussion, Department of Meteorology, University of Maryland, http://www.meto.umd.edu/~ryan/aug2125.htm, 1999.

Saxeena, Pradeep and Glen Cass, "Designing Atmospheric Experiments to Enable Estimation of Source-Receptor Relationships for Fine Particles," Proceedings of the PM Measurements Research Workshop, EPA Report No. 4, Chapel Hill, North Carolina, pp. 19-26, July 22-23, 1998.

Science and Engineering Services, Inc., Micro Pulse Lidar Instruction Manual, Rev 2, 1996.

Sillman, Sanford, "Tropospheric Ozone: The Debate Over Control Strategies," Annual Review of Energy and the Environment, Volume 18, Annual Review Inc.: Palo Alto, CA, pp. 31-55, 1993.

Stephens, Timothy D., "Bistatic Lidar Measurements of Lower Tropospheric Aerosols," Doctor of Philosophy Thesis for Penn State University, Department of Electrical Engineering, May, 1996.

Walcek, Chris J, and Hong-H. Yuan, "Calculated Influence of Temperature-Related Factors on Ozone Formation Rates in the Lower Troposphere," Journal of Applied Meteorology, Vol. 34, pp. 1056-1065, 1994.

Wiegner, Matthias, and Volker Freudenthaler, "Two Approaches to Derive Aerosol Extinction Coefficient Profiles from Backscatter Lidar Measurements," Proceedings of the Nineteenth International Laser Radar Conference, NASA Langley Research Center, Hampton, VA, NASA Conf. Publ. 207671, pp. 127 – 129, July 1998.

Zhang, Jian and S. Trivikrama Rao, "The Role of Vertical Mixing in the Temporal Evolution of Ground-Level Ozone Concentration," Journal of Applied Meteorology, 38, 1999.